Memoirs of the School of Engineering, Nagoya University
Vol.49, No.1 (1997)

ON THE PROPERTIES AND BEHAVIOR OF RADON AND ITS DAUGHTERS IN THE ATMOSPHERE

Yukimasa IKEBE, Takao IIDA, Michikuni SHIMO*
and Tetsuya SAKASHITA*

Department of Nuclear Engineering

(Received June 6, 1997)

Abstract

Research works on the atmosphere radon and its' daughters have been carried out. The correlations among the concentrations of unattached ^{218}Po and ^{218}Po ions, the number and size of condensation nuclei, and the effective attachment coefficients were clarified. The variations of radon and thoron concentrations were analyzed in relation to the wind speed and turbulent diffusivity. Outdoor and indoor ^{222}Rn concentrations in Japan and China have been surveyed using passive electrostatic integrating ^{222}Rn monitors. The annual mean outdoor ^{222}Rn concentrations ranged from 2.4 to 9.7 Bq m^{-3} and 4.8 to 14.6 Bq m^{-3} in Japan and China, respectively. The ratios of indoor and outdoor ^{222}Rn concentrations were about 2 to 3. Outdoor ^{222}Rn concentrations were measured continuously with ectrostatic radon monitors at six locations in Japan and China. The ^{222}Rn concentrations at Nagoya, Kasugai, Toki, Beijing and Fuzhou showed a diurnal variation clearly in autumn. At Kanazawa, the clear diurnal variation appeared in summer. An analytical model of one layer long range transport of "background component" of ^{222}Rn was proposed using air mass trajectory technique. This model could explain the temporal variation of background component of ^{222}Rn. In addition, a three-dimensional numerical simulation model was developed for calculating the temporal variation of ^{222}Rn. The variation of observed ^{222}Rn concentration agreed with that of calculated one.

Keywords: radon, thoron, radioactive ion, temporal variation, diurnal variation, passive method, outdoor and indoor ^{222}Rn concentration, diffusion equation, numerical simulation.

* National Institute of Radiological Sciences

Contents

1. Properties of Radon Daughters

1.1 Introduction

^{218}Po(RaA) is produced by α-decay of ^{222}Rn. At the time of formation, RaA is an unattached atom in the atmosphere which, after a short time, attaches to an aerosol particle forming attached RaA. A fraction of the unattahced RaA is ion and the rest is neutral.

Many authors[1,2] have studied the natural radioactivity in the atmosphere; in particular, the time variations of concentrations of radioactive substances, the local anomaly on land, and the relation between concentrations of radioactive substances and meteorological elements have been fairly well studied. However, the researches on the properties of natural radioactive ions are considerably few[3,4,5]. According to Chamberlain and Dyson[6], the most fundamental form of naturally occurring radioactive ions is the RaA (^{218}Po) ion of which mobility, denoted by k, is $2.2\,cm^2s^{-1}volt^{-1}$. In the previous paper[7], the present authors clarified that the radioactive nuclides carried by radioactive ions (k=$2.2\,cm^2s^{-1}volt^{-1}$) are mainly RaA. In this chapter, we describe first the interaction between RaA ions and condensation nuclei.

When we estimate the lung dose from radon and thoron decay products, we must take into account that a considerable number of unattached atoms may be deposited in the trachea and the brochial region, while the attached atoms are mainly deposited in the pulmonary region[8,9]. In addition, ICRP Publication 32[10] indicates that for the special case of inhaled unattached radon daughters a considerably higher dose is given to the bronchial than the pulmonary epithelium. It is therefore important to know the unattached fraction. In this chapter, we also describe the research for unattached fraction of radon daughters.

1.2 The interactions between RaA ions and condensation nuclei

1.2.1 Measurement

The following simultaneous measurements were carried out from July, 1964 through Feb., 1967 at various stations in the central area of Japan;

concentration of RaA ions, n_A (cm^{-3})
concentration of condensation nuclei, Z (cm^{-3})
rate of RaA ion production, q_A ($cm^{-3}\,s^{-1}$)
and diffusion coefficient of condensation nuclei, D ($cm^2\,s^{-1}$).

1.2.2 Instruments used for measurements

The instruments used for the present work are as follows:

(1) Concentration of RaA ions (n_A)

The apparatus used for collecting radioactive ions is shown in Fig. 1-1. The diameter and

the length of the flow tube are 25 cm and 250 cm, respectively. A copper wire of 0.055 cm in diameter and 200 cm in length is supported by insulators coaxially in the flow tube and is maintained at negative potential of 225 volts. The flow tube is always grounded. The air is drawn through the flow tube at rate of 200 cm s^{-1}. From the values of the potential difference and the velocity of air-flow used here, the critical mobility of radioactive ions trapped on the wire is calculated to be 2.2 $cm^2 s^{-1} volt^{-1}$. The radioactive ions are collected for one hour, and at the end of the collection period, the wire is wound upon a flat spool for activity counting. A ZnS scintillation counter is used for alpha-counting, and counted values are recorded for 90 minutes after the end of the collection.

It was clarified that the radioactive nuclides trapped on the wire are mainly RaA[7]. Then the time variation of alpha-disintegration of the wire may be expressed by the following formula;

$$
\begin{aligned}
I_A &= \lambda_A N_A + \lambda_C N_C \\
&= \varepsilon Q n_A \left[\frac{\lambda_B \lambda_C (1 - e^{-\lambda_A T})}{(\lambda_B - \lambda_A)(\lambda_C - \lambda_A)} (e^{-\lambda_A t} - e^{-\lambda_C t}) \right. \\
&\quad - \frac{\lambda_C \lambda_A (1 - e^{-\lambda_B T})}{(\lambda_C - \lambda_B)(\lambda_B - \lambda_A)} (e^{-\lambda_B t} - e^{-\lambda_C t}) \\
&\quad + \{ (1 - e^{-\lambda_C T}) + \frac{\lambda_A \lambda_C}{(\lambda_B - \lambda_A)(\lambda_C - \lambda_B)} \\
&\quad \times (e^{-\lambda_B T} - e^{-\lambda_C T}) - \frac{\lambda_B \lambda_C}{(\lambda_B - \lambda_A)(\lambda_C - \lambda_A)} \\
&\quad \left. \times (e^{-\lambda_A T} - e^{-\lambda_C T}) \} e^{-\lambda_C t} + (1 - e^{-\lambda_A T}) e^{-\lambda_A t} \right]
\end{aligned}
\tag{1-1}
$$

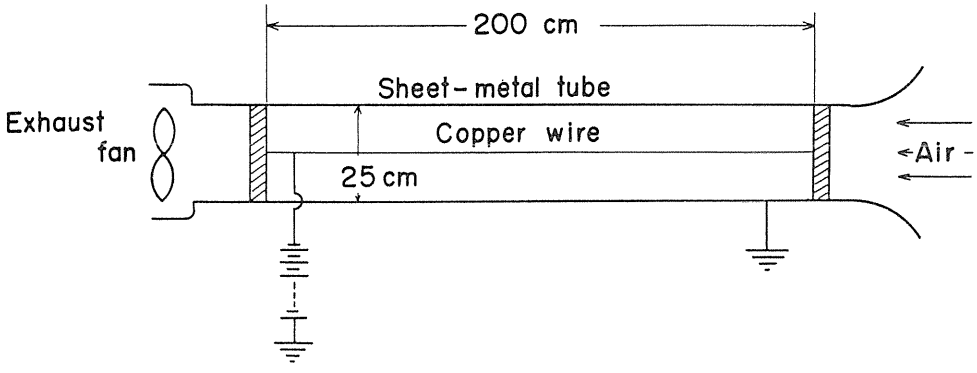

Fig. 1-1 The apparatus used for collecting RaA ions (Negative Wire).

where

I_α	: alpha-disintegration rate at time t (dps)
ε	: collection efficiency for RaA ions
Q	: flow-rate ($cm^3 s^{-1}$)
n_A	: concentration of RaA ions (cm^{-3})
N_A and N_C	: numbers of RaA and RaC atoms on a wire respectively
λ_A,λ_B and λ_C	: decay constants of RaA, RaB, and RaC respectively (s^{-1})
T	: collection time(s).

Substituting the values $\varepsilon=1$, $Q=\pi(\frac{25}{2})^2\times 200\ cm^3 s^{-1}$, $\lambda_A=3.79\times10^{-3}s^{-1}$, $\lambda_B=4.31\times10^{-4}s^{-1}$, $\lambda_C=5.86\times10^{-4}s^{-1}$, and T=7,200s into formula 1-1, and using 0.080 as the value of counting efficiency of the scintillation counter, we can estimate the concentration of RaA ions (n_A) in the air from the counting rate.

(2) Concentration of condensation nuclei (Z)

A Pollak photoelectric nucleus counter was used for the present work. The calibration curve obtained by Nolan[11] was used for estimating the concentration of condensation nuclei from the measured value of extinction.

(3) Diffusion coefficient of condensation nuclei (D)

The diffusion battery method[12,13] was used for measuring diffusion coefficient of condensation nuclei. A metal diffusion battery with ten channels was used. The diffusion coefficient of condensation nuclei was estimated by using Gormley's formulae[13]. A particle diameter ($2r$) corresponding to a value of diffusion coefficient was calculated by using Stokes-Cunningham formula.

(4) Rate of RaA ion production (q_A)

Although it is well known that positively charged RaA atoms are present in the atmosphere, it has not been perfectly clarified how many per cent of RaA atoms are positively charged and how many per cent are neutral. We denote the charged fraction of RaA atoms produced by α-decay of Rn-222 by f, and the fraction of neutral RaA atoms by (1-f). Then we may estimate the rate of radioactive (RaA) ion production from the concentration of radon gas in the air:

$$q_A = f q_{Rn} = f\lambda_{Rn} n_{Rn} \tag{1-2}$$

where

f	: charged fraction of RaA atoms produced by α-decay of Rn-222
q_{Rn}	: rate of RaA atom production ($cm^{-3}s^{-1}$)
λ_{Rn}	: decay constant of Rn-222 (s^{-1})
n_{Rn}	: concentration of Rn-222 (cm^{-3}).

In the present work, the concentration of Rn-222 was measured by means of the charcoal trap method or the filter pack method.

1.2.3 Results of measurements

(1) Mean life of RaA ions

The mean life of RaA ions is given by the following relation;

$$\theta_A = \frac{1}{\beta_A Z} \tag{1-3}$$

where

θ_A : mean life of RaA ions(s)

β_A : effective attachment coefficient between RaA ions and condensation nuclei ($cm^3 s^{-1}$).

In the case of RaA ion equilibrium, the following relation may be given:

$$\beta_A = \frac{q_A}{n_A Z} \tag{1-4}$$

The rate of RaA ion production (q_A) cannot be directly measured. We can determine only the value of $q_{Rn} = q_A/f$, β_A/f, or $f\theta_A$. However, as is described by Ikebe[14], the value of f is estimated to be about 0.26. The average mean life of RaA ions is about 12 sec on the campus of Nagoya Univ., but is rather long at Mt. Norikura (36 s), Toki (50 s), and Tadeshina (24 ~ 37 s).

(2) The correlation between the concentration of RaA ions and that of condensation nuclei

According to the formula (1-4), n_A/q_A is expected to be inversely proportional to Z, if we assume β_A to be constant. In actual, the value of β_A is considered to be mainly controlled by the size of condensation nuclei ($2r$), and the time variation of r, hence β_A are remarkably wide. Fig. 1-2 shows the correlation between n_A/q_A and Z. The data shown in the figure is classified into five groups according to the value of D measured simultaneously. In each group, the value of D, hence β_A is rather constant. As is shown in this figure, n_A/q_A is almost inversely proportional to Z. Thus, if we take the variation of D into consideration, the correlation among n_A, Z, and q_A is expressed by the simple formula; $q_A = \beta_A n_A Z$.

(3) The effective attachment coefficient

The effective attachment coefficient between RaA ions and condensation nuclei (β_A) may be estimated from the formula (1-4). β_A is considered to be a function of the diffusion

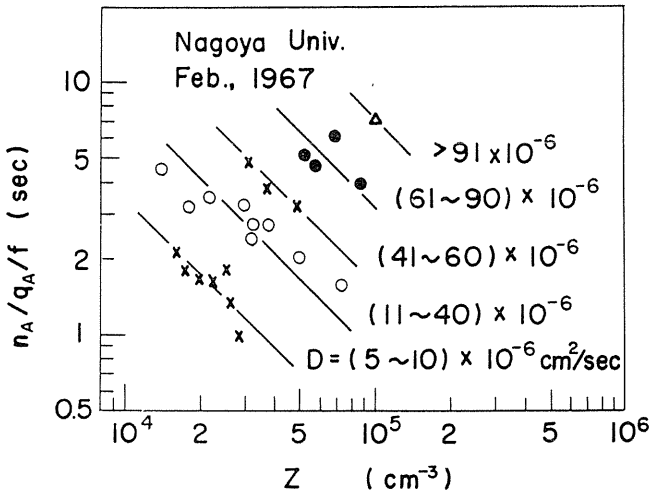

Fig. 1-2 The correlation between $n_A/(q_A/f)$ and the concentration of condensation nuclei. Data is classified according to the value of D.

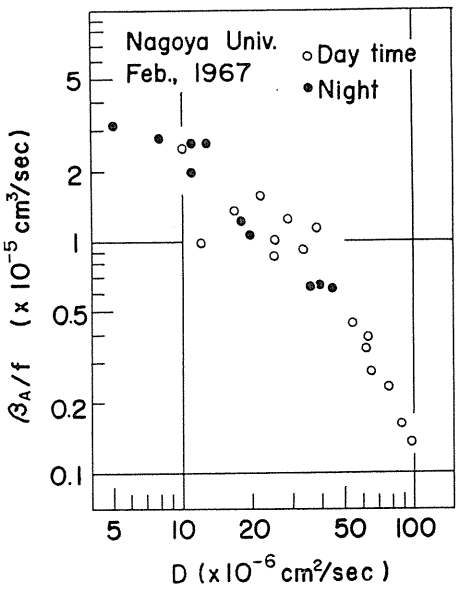

Fig. 1-3 The correlation between the attachment coefficient of RaA ions (divided by f) and the diffusion coefficient of condensation nuclei.

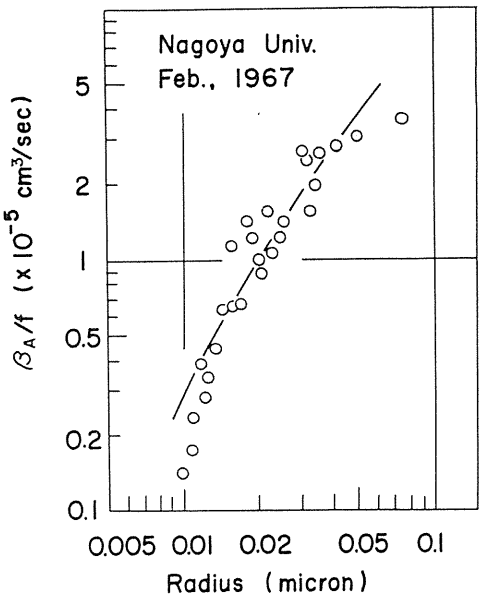

Fig. 1-4 The correlation between the attachment coefficient of RaA ions (divided by f) and the radius of condensation nuclei.

coefficient of nuclei (D). Fig. 1-3 shows the correlation between β_A/f and D measured on the campus during Feb., 1967. As is shown in this figure, β_A/f correlates fairly well with D. The average diameter of condensation nuclei ($2r$) may be calculated by using Stokes-Cunningham formula. In Fig. 1-4 the correlation between β_A/f and r is shown. Similar correlations were also obtained at Tadeshina, in Aug., 1966.

According to Keefe and Nolan[15], the effective attachment coefficient between small ions and nuclei (b) is expressed theoretically as a function of that between ions and uncharged nuclei (η_0), and η_0 is given as follows:

$$\eta_0 = \frac{4\pi r D_0(1+\sqrt{\pi y})}{1+\frac{4D_0}{rC}} \tag{1-5}$$

where

r : radius of the nucleus (assumed spherical)
C : average speed of the small ions
D_0 : diffusion coefficient of the small ions

$$y = \frac{e^2}{2rkT} \left(= \frac{2.88\times10^{-6}}{r} \right) \quad \text{for a temperature of 17°C)}$$

where e is electronic charge, T is absolute temperature, and k is Boltzmann's constant.

Our results of observations of small ions measured simultaneously together with RaA ions suggested the excess of uncharged nuclei (or the lack of charged nuclei) in the atmosphere during the observation period[16]. In this case, b approaches η_0.

In this case of RaA ion, D_0=0.054 cm^2s^{-1} and C=1.75×10^4 $cm\,s^{-1}$. Inserting these values into formula (1-5), we obtain η_0 as a function of r. The solid line in Fig. 1-4 represents η_0 (arbitrary unit). The measured values shown in the figure agree fairy well with the solid line in the range of r larger than 0.015 μm.

Lassen and Rau[17] obtained a similar formula, but without the image term, to describe the attachment of ThB atom to aerosol particle. Our measured values seem to agree well with the Lassen and Rau's theory in the range of r smaller than 0.03 μm.

1.3 Measurements of free RaA

1.3.1 Measurements

The short-lived radon daughters were sampled on a filter, and α particles were counted using ZnS(Ag) scintillation equipment. The equilibrium equivalent RaA concentration, Q_A was obtained by analyzing a single count of the filter assuming radioactive equilibrium between radon daughters. The wire screen method[18] was used for measuring the unattached concentration of RaA, Q_A^f. We used an ordinary filter holder where a wire screen was used instead of a filter. In this case the RaA activity was obtained assuming no RaB and RaC on the wire screen. The unattached fraction f_A is presented as follows[19];

$$f_A = \frac{Q_A^f}{Q_A} = \frac{\lambda_A}{\lambda_A + \beta Z} \tag{1-6}$$

where λ_A is the decay constant of RaA nuclide(s), β is the attachment coefficient of unattached atom to aerosol particles ($cm^3.s^{-1}$) and Z is the aerosol particle concentration (cm^{-3}). The quantity β Z indicates the attachment rate of an unattached atom to an aerosol particle[20].

1.3.2 Results of measurements

In Fig. 1-5, the result of measurements of f_A is shown. In the figure, r is the radius of atmospheric aerosols determined by using a diffusion battery. Inverse correlation between f_A and Z is seen. The observed values agree to a considerable degree with the theoretical curve calculated from Fuch's theory[21]. A detailed discussion of this relation is included in a previous paper by Shimo et al[9].

1.4 Conclusion

To clarify the interaction between RaA ions and condensation nuclei, simultaneous measurements of the concentration of RaA ions (n_A), radon-222, and condensation nuclei (Z) were carried out at several stations. In some occasions, the diffusion coefficients of nuclei (D) were also measured. It was found that the correlation among them may be well expressed by the simple formula; $q_A=\beta_A n_A Z$. The correlation between β_A and D (or radius of nuclei) was also obtained.

For evaluating the unattached fraction f_A (fraction of RaA atoms unattached on aerosols) in the open air, the total activities and the unattached activities of RaA atmos have been measured in various environments. The observation of the number concentration Z and mean radius of aerosols have also been carried out simultaneously. It is shown that the unattached fraction decreases with increase of the aerosol particle concentration and that an observed unattached fraction agrees with the calculated one.

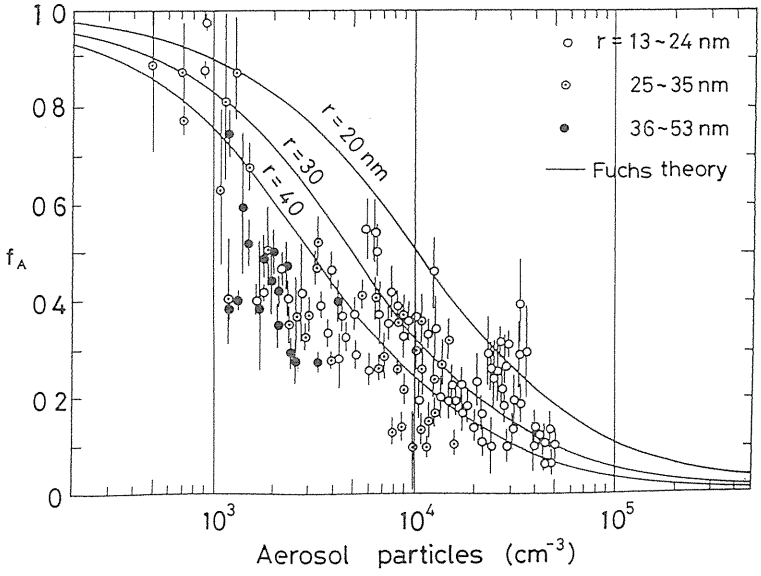

Fig. 1-5 Variation of the unattached fraction as a function of aerosol particles. r=radius of aerosol particles. Standard error of aerosol particles is less than few per cent.

2. Analysis of the Variation of Radon and Thoron Concentration in Relation to the Wind Speed and Turbulent Diffusivity

2.1 Introduction

^{222}Rn (radon, Rn) and ^{220}Rn (thoron, Tn) diffuse continuously from the ground surface to the atmosphere. These radioactive emanations are transported upwards by turbulent diffusion in the atmosphere.

There have been numerous researches for the relation between Rn and Tn concentrations and turbulent diffusivity of the air (K). The vertical distributions of Rn and Tn have been calculated by assuming various functional forms of K with respect to altitude[25-31]. On the contrary, several researches[32-35] calculated the mean value of K between two altitudes from Rn measurements, assuming K to be constant.

In this chapter, analytical solutions of the diffusion equation obtained by assuming linear increase of the diffusion coefficient with respect to altitude are presented. The relationships between the concentrations of the emanations and wind speed are also obtained theoretically, and are compared with those obtained by field measurements. We also report the evaluation of the vertical profiles of the turbulent diffusivity from observed Tn profiles.

2.2 Vertical profiles of Rn and Tn concentrations

2.2.1 Analytical solutions of the diffusion equation

The equilibrium vertical profiles of Rn (^{222}Rn) and Tn (^{220}Rn) for steady-state conditions at a constant exhalation rates of Rn and Tn can be obtained from the following differential equation;

$$\frac{d}{dz}\left(K\frac{dn}{dz}\right)-\lambda n=0 \tag{2-1}$$

where

n : concentration of Rn or Tn at altitude z (Bq cm^{-3})

K : diffusion coefficient (cm^2s^{-1})

λ : radioactive decay constant of Rn or Tn (s^{-1}).

The diffusion coefficient K is quite valiable with altitude. In the turbulent boundary layer near the ground surface, K is approximately expressed by the following linear law of z;

$$K=a+bz$$

where

a : molecular diffusion coefficient (cm^2s^{-1})

b : turbulent diffusion coefficient at a unit altitude (cm^2s^{-1}).

Above the boundary layer, K seems to be rather constant. In the present work, we assume two types of K-profiles;

$$\text{Case 1 ;} \qquad K=a+bz \quad for \quad 0\le z\le\infty \tag{2-2}$$

$$\text{Case 2 ;} \qquad \left.\begin{aligned} &K=a+bz \quad for \quad 0\le z\le H\\ &K=a+bH \quad for \quad z\ge H \end{aligned}\right\} \tag{2-3}$$

Substituting (2-2) into (2-1), we obtain as the diffusion equation

$$(a+bz)\frac{d^2n}{dz^2}+b\frac{dn}{dz}-\lambda n=0\,. \tag{2-4}$$

Introducing a variable $y=\sqrt{a+bz}$, we obtain from (2-4)

$$\frac{d^2n}{dy^2}+\frac{1}{y}\left(\frac{dn}{dy}\right)-\frac{4\lambda}{b^2}n=0\,. \tag{2-5}$$

The general solution of the equation (2-5) is

$$\begin{aligned} n&=AI_0\left(\frac{2}{b}\sqrt{\lambda}y\right)+BK_0\left(\frac{2}{b}\sqrt{\lambda}y\right)\\ &=AI_0\left(\frac{2}{b}\sqrt{\lambda(a+bz)}\right)+BK_0\left(\frac{2}{b}\sqrt{\lambda(a+bz)}\right) \end{aligned} \tag{2-6}$$

where I_0 is the modified Bessel function of the first kind of order zero, and K_0 is the modified Bessel function of the second kind of order zero.

Now we shall introduce the following boundary conditions: (i) Rn and Tn have properties of radioactive decay. Consequently,

$$n(z\to\infty)\to 0\,. \tag{2-7}$$

(ii) The total activity of Rn or Tn in a vertical air column is equal to the exhalation rate at the ground surface. Therefore,

$$\int_0^\infty \lambda n dz = E \tag{2-8}$$

where E is the exhalation rate of Rn or Tn atom from the ground surface (Bq $cm^{-2}s^{-1}$). From the condition (i),

$$A = 0 . \tag{2-9}$$

Inserting (2-6) and (2-9) into the condition (ii), we obtain

$$\lambda B \int_0^\infty K_0\left(\frac{2}{b}\sqrt{\lambda(a+bz)}\right) dz = E . \tag{2-10}$$

Putting $\int_0^\infty K_0\left(\frac{2}{b}\sqrt{\lambda(a+bz)}\right) dz = I$ and introducing a new variable $x = 2\sqrt{\lambda(a+bz)}/b$, we obtain

$$I = \frac{b}{2\lambda}\int_{\frac{2\sqrt{\lambda a}}{b}}^\infty K_0(x)x dx = \frac{-b}{2\lambda}\left[xK_1(x)\right]_{\frac{2\sqrt{\lambda a}}{b}}^\infty \tag{2-11}$$

where K_1 is the modified Bessel function of the second kind of first order. It is easily proved that $\lim_{x\to\infty} xK_1(x) = 0$. Then we obtain from (2-10) and (2-11)

$$B = E/\sqrt{\lambda a}K_1\left(\frac{2\sqrt{\lambda a}}{b}\right). \tag{2-12}$$

Inserting (2-9) and (2-12) into (2-6), we obtain as the solution of the equation (2-1)

$$n = EK_0\left(\frac{2}{b}\sqrt{\lambda(a+bz)}\right)/\sqrt{\lambda a}K_1\left(\frac{2\sqrt{\lambda a}}{b}\right). \tag{2-13}$$

This result is in accordance with the solution obtained by Wormell[36] (1965, unpublished, refered by Crozier and Biles) and by Israel et al[37] by means of a different method.

For case 2, the solution of equation (2-3) may be obtained by similar way;

$$n_{\mathrm{I}} = B\{NI_0(x) + K_0(x)\} \quad x \leqq H \tag{2-14}$$

$$\text{and} \quad n_{\mathrm{II}} = BMe^{-\sqrt{\lambda/K_H}(Z-H)} \quad x > H \tag{2-15}$$

where $N \equiv \dfrac{K_1(x_H) - K_0(x_H)}{I_0(x_H) + I_1(x_H)}$, $M \equiv \dfrac{1}{x_H}\cdot\dfrac{1}{I_0(x_H) + I_1(x_H)}$

$x_H \equiv 2\sqrt{\lambda(a+bH)}$,

$$B = 2E \cdot \left\{ bN[xI_1(x)]_{x_0}^{x_H} - b[xK_1(x)]_{x_0}^{x_H} + 2M\sqrt{\lambda K_H} \right\}^{-1}$$

and I_1 is the modified Bessel function of the first kind of first order.

2.2.2 *Results of calculation*

Vertical profiles of Rn and Tn were calculated by using the solutions described above. In the present work, we used the following values of constants: a=0.054 cm^2s^{-1} for Rn and Tn, λ=2.10×$10^{-6}s^{-1}$ for Rn, and λ=1.30×$10^{-2}s^{-1}$ for Tn. As the exhalation rate we supposed E_A=1 Rn or Tn atom/cm^2.

Case 1 ; $K = a + bz \ (0 \leq z \leq \infty)$

Inserting these values of constants into (2-13), we can obtain Rn and Tn profiles for the case of K=a+bz. The calculated profiles of Rn and Tn are shown in Figs. 2-1 and 2-2, respectively.

Case 2 ; $\left.\begin{array}{l} K = a + bz \ (0 \leq z \leq H) \\ K = a + bH \ (z \geq H) \end{array}\right\}$

In the present work, the value of H was taken as 200 m for each value of b.

With respect to Tn, the results of calculation for case 2 coincide quite well with that shown in Fig. 2-2 which was calculated for case 1. Tn profiles shown in Fig. 2-2 coincide also with some of those obtained by Jacobi and Andre who assumed several typical K profiles similar to the present work. These circumstances seem to show that the value of K above 200 m altitude do not affect Tn profiles below about 10 meters.

Fig. 2-3 shows the result of calculation for Rn.

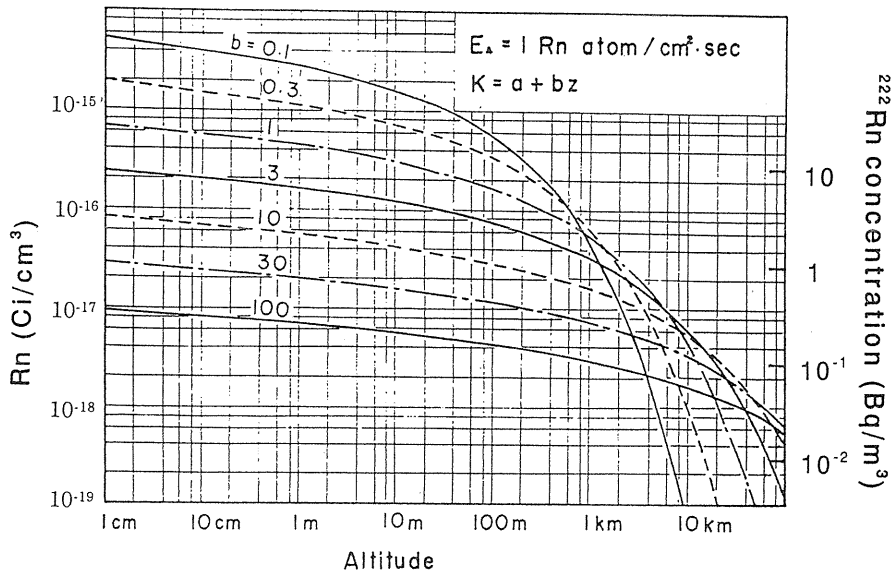

Fig. 2-1 Vertical profile of ^{222}Rn (radon) for Case 1 ; $K = a + bz \ (0 \leq z \leq \infty)$.

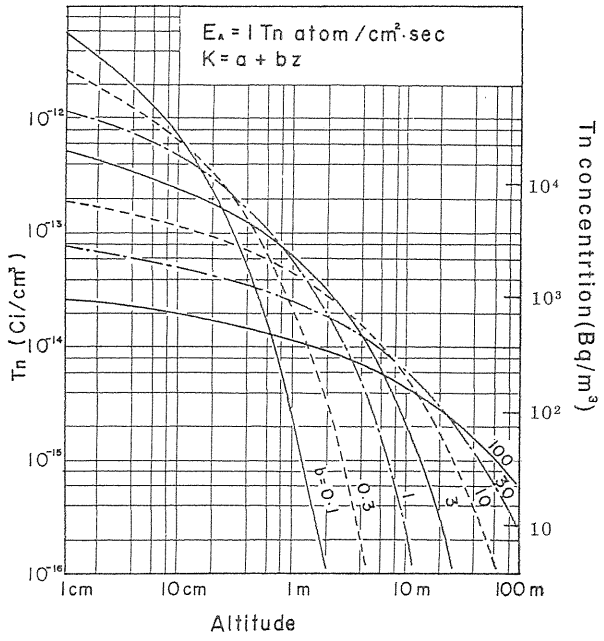

Fig. 2-2 Vertical profile of ^{220}Rn (thoron) for Case 1 ; $K = a + bz\ (0 \leq z \leq \infty)$. This profiles agree quite well with those for case 2.

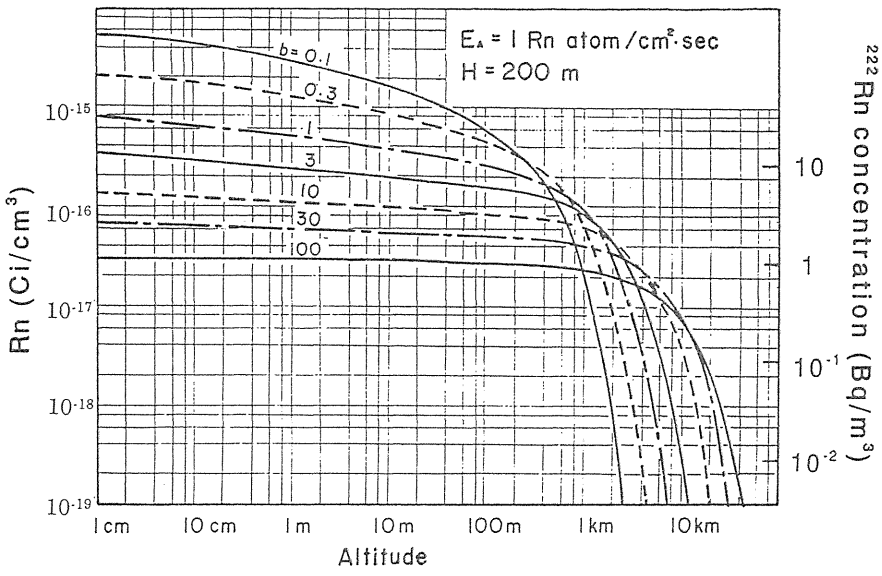

Fig. 2-3 Vertical profile of ^{222}Rn (radon) for case 2 ; $\left.\begin{array}{l} K = a + bz\ (0 \leq z \leq 200m) \\ K = a + bH\ (z \geq H = 200m) \end{array}\right\}$

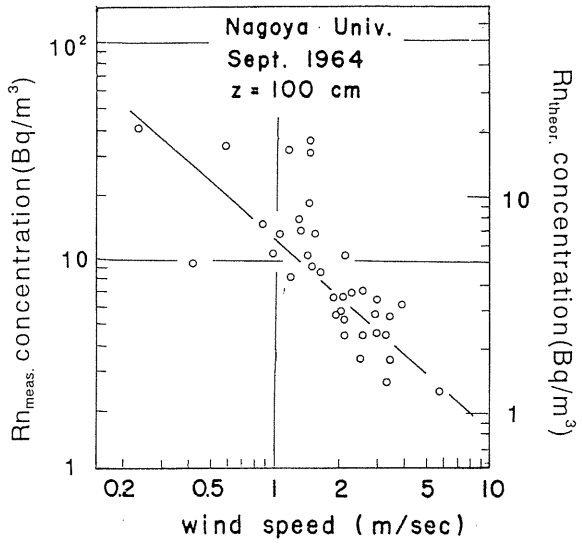

Fig. 2-4 Correlation between the concentration of ^{222}Rn (radon, z=1 m) and wind speed (z=1 m) obtained on the campus. Solid lines represent the theoretical relationships for case 1; (Z_0=0.2 cm).

2.3 Relation between the concentration of Rn and wind speed

In general, concentrations of Rn and Tn in the atmosphere vary widely with a change of time. For example, the concentration of Rn at 1 meter above the ground surface measured on the campus of this university had a range of values from 0.4 Bq m^{-3} to 35 Bq m^{-3}, varying considerably from day to day. The main cause of the time variation of Rn and Tn concentrations seems to be change of vertical turbulent diffusivity or wind speed.

Fig. 2-4 shows some example of the correlations between the Rn concentration measured on the campus and the wind speed at 1 meter above the ground. As shown in the figure, negative correlation is apparent.

The relationship may be found theoretically as follows: Under neutral condition, the vertical distribution of mean wind speed near the ground is given by the logarithmic profile[38];

$$u(z) = \frac{u_*}{k} ln \frac{z}{z_0} \tag{2-16}$$

where

$u(z)$: wind speed at altitude z (cm s^{-1})
u_* : frictional velocity (cm s^{-1})
k : von Kárman constant ≅ 0.41

and z_0: roughness length (cm).

Assuming the vertical turbulent diffusion coefficient of Rn and Tn, denoted by K(z), to be equal to that of momentum, we can express K(z) as

$$K(z) = ku_* z . \tag{2-17}$$

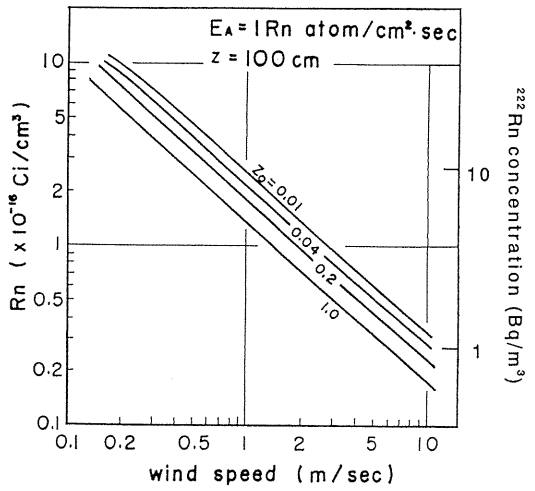

Fig. 2-5 Relationship between the concentration of ^{222}Rn (radon z=1 m) and wind speed (z=1 m) estimated for case 1.

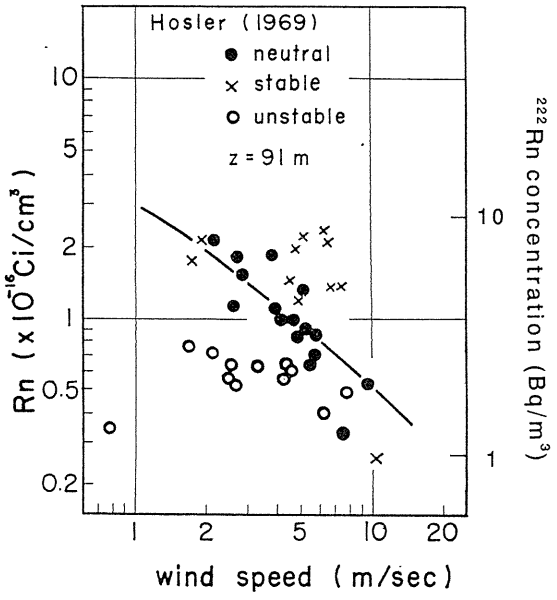

Fig. 2-6 Relation between the concentration of ^{222}Rn (radon, z=91 m) and wind speed (z=91 m) obtained from Hosler's data. The solid line represents the theoretical relationship for case 1 (z_0=0.2 cm).

If $u(z_1)$ is given, we can estimate $K(z_1)$ from (2-16) and (2-17). Then we can estimate corresponding $n(z_1)$ from Fig. 2-1. Thus the relationship between $n(z_1)$ and $u(z_1)$ may be obtained. Fig. 2-5 shows the relationships between the Rn concentrations and wind speed. In the figure, the value of E_A is taken as 1 atom $cm^{-2}s^{-1}$, and the value of z_1 is taken as 1 m. The solid line in Fig. 2-4 represents the theoretical relationship between the Rn concentration and wind speed. In the figure, z_0 is taken as 0.2 cm[39]. The observed data correlate fairly well with the theoretical line.

Comparing the theoretical line for E_A=1 atom cm^2s^{-1} with observed data (for unknown exhalation rate), we can estimate exhalation rates of Rn. The exhalation rate of Rn is estimated to be 44 m Bq $m^{-2}s^{-1}$ which seems reasonable as compared with the results obtained by several researchers[40-44,33].

In order to see the effect of the stability of the atmosphere upon the dispersion of the observed data of Fig. 2-4, data obtained by Hosler[33] were analyzed by the similar method described above. Fig. 2-6 shows the results. The data obtained on the neutral condition agree well with the theoretical relation, whereas those obtained on the stable and unstable condition don't agree. Thus the stability of the atmosphere seems to much affect on the relation. For neutral condition, the assumption of the constant exhalation rate seems to be correct.

2.4 Estimation of vertical turbulent diffusivity from Tn profiles

2.4.1 Measurements of Tn profiles

Field measurements were conducted by using an ionization chamber at two sites on the university campus; in the green belt where the ground surface in covered with lawn (lawn area, 61 m×91 m) and on the bare soil (soil area, 61 m×100 m)[14]. Measurements were made in the daytime from Aug. to Nov. 1968. Among the Tn profiles obtained during the measuring period, those which satisfy the following three conditions are chosen in the present work as some examples of Tn profiles: (1) wind direction; N ~ NW, (2) fairly constant wind speed,

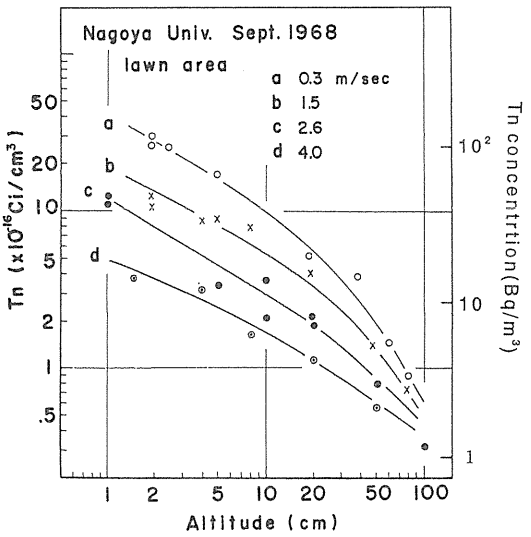

Fig. 2-7 Vertical profile of thoron concentration measured on the lawn area of the campus. (a) Sept. 3 (u=0–0.5 m s^{-1}); (b) Sept. 2 (0.7–2.0); (c) Sept. 6 (2.0–3.2); (d) Aug. 31 (3.2–6.0).

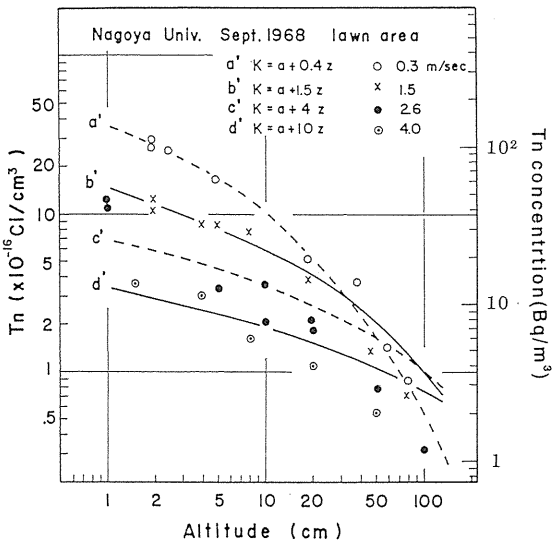

Fig. 2-8 Comparison of the observed points of thorn obtained on the lawn area with calculated thoron profiles by assuming K=a+bz.

and (3) dry ground surface. The measurements were made at the leeward (east) edge of each site.

Fig. 2-7 shows Tn profiles measured above the lawn area. In the figure, measured points are classified into four groups according to the date of measurements. As is shown in the figure, four Tn Profiles may be drawn according to the wind speed (u) at 1 m above the ground. The profiles seem to be fairly similar to those obtained by Crozier & Biles[45]. The curves drawn in Fig. 2-8 among the plotted observed points are theoretical ones calculated from equation (2-13) for a constant exhalation rate.

Although observed points for $u=0.3\,m\,s^{-1}$ rather seem to agree with calculated profile for K=a+0.4 z, those for $u=2.6\,m\,s^{-1}$ and $4.0\,m\,s^{-1}$ do not agree with calculated profiles. These discrepancies suggest that the diffusivity K in the atmosphere near the ground cannot be expressed strictly by K=a+bz. Therefore, in the following section we attempt to evaluate K profiles from observed Tn profiles.

2.4.2 Estimation of Tn exhalation rate

To evaluate K profiles from observed Tn profiles, we must evaluate Tn exhalation rate (E_0) at the observation sites. Recently methods for the direct measurement of Tn exhalation rates have been developed by several researchers. However, it is as yet impossible to measure E_0 directly taking into consideration of the effect of the wind speed. In the present work, we estimate E_0 indirectly as described in section (2-3). Thus the exhalation rate of Tn above the lawn area was evaluated to be $340\,m\,Bq\,m^{-2}\,s^{-1}$.

2.4.3 Estimation of K profiles from Tn Profiles

In the present work, K profiles are evaluated from observed Tn profiles as follows: Integrating the diffusion eq. (2-1) for steady state condition, we obtain

$$\left[K\frac{dn}{dz}\right]_{z_3}^{z} = \int_{z_3}^{z} \lambda n dz . \tag{2-18}$$

Then K(z) may be given by

$$K(z) = \left\{K(z_3)\left(\frac{dn}{dz}\right)_{z_3} + \lambda\int_{z_3}^{z} n dz\right\} / \left(\frac{dn}{dz}\right)_z . \tag{2-19}$$

Now Tn flux E at altitude z may be given by

$$E = -K\frac{dn}{dz} . \tag{2-20}$$

Then

$$K(z) = \left\{-E(z_3) + \lambda\int_{z_3}^{z} n dz\right\} / \left(\frac{dn}{dz}\right)_z . \tag{2-21}$$

From observed Tn profiles, we can evaluate

$$(dn/dz)_z , \quad (dn/dz)_{z_3} \quad \text{and} \quad \int_{z_3}^{z} n dz .$$

In this work z_3 is taken as 3 cm, and E(3) is estimated in each profiles as

$$\frac{E(3) - E(0)}{3} = -\lambda n(1.5) . \tag{2-22}$$

Then we can evaluate K(z) from the formula (2-21).
Fig. 2-9 shows the K profiles on the lawn area estimated from Tn profiles shown in Fig. (2-7) using eqs. (2-21) and (2-22). As is shown in the figure, estimated K profiles somewhat differ from $K \cong bz$. The estimated K profiles may be expressed well by an experimental formula

$$K(z) = \alpha z^{\beta} . \tag{2-23}$$

The values of α and β are shown in Table 2-1. β takes the values from 1.3 to 1.5. The discrepancies between the diffusivity K_{Tn} estimated from Tn profiles and that K_M calculated from the Rossby relation (2-16) were discussed from the view point of the stability of the atmosphere[14].

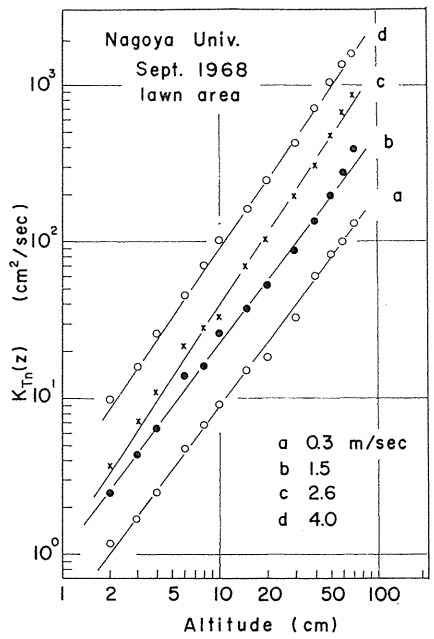

Fig. 2-9 Vertical K profiles on the lawn area estimated from thoron profiles shown in Fig. (2-7).

Table 2-1 $K(z)=\alpha z^{\beta}$ profiles estimated from thoron profiles.

Profile	Date	α	β
a	Sept. 3	0.40	1.35
b	Sept. 2	1.0	1.3
c	Sept. 6	1.1	1.5
d	Aug. 31	3.0	1.4

2.5 Conclusion

The vertical distributions of Rn and Tn were obtained analytically under some conditions of the diffusion coefficient with respect to altitude. The theoretical relationships between the concentration of the emanations and wind speed were compared with those obtained by field measurements, and fairly good agreements were obtained. The main cause of the dispersion of the data seems to be the stability of the atmosphere.

Field measurements of the vertical Tn profiles were carried out on the campus. Comparing the observed Tn profiles with those calculated by assuming K=a+bz, some discrepancies were found between them.

Estimations of K profiles from observed Tn profiles were made. It was found that the estimated K profiles may be expressed well by an experimental formula; $K(z)=\alpha z^{\beta}$.

3. A Survey of Outdoor and Indoor ^{222}Rn Concentrations by Passive Method in Japan and China

3.1 Introduction

Many type of passive ^{222}Rn monitors[51,52,53] have been widely used for the survey of time average indoor ^{222}Rn concentrations. To evaluate lung dose precisely due to inhalation of ^{222}Rn and its daughters, it is necessary to measure also mean ^{222}Rn concentrations in various outdoor environments. However, the measurements of regional distribution of outdoor ^{222}Rn concentration have hardly been carried out due to lack of high sensitive passive ^{222}Rn monitor[54]. The information on the regional distribution of ^{222}Rn concentration and its time variation is also important to study ^{222}Rn in relation to ^{226}Ra concentrations in soil, ^{222}Rn exhalation, geographical features, and its behavior in the atmosphere.

The authors[55] studied and developed a new type of passive electrostatic integrating ^{222}Rn monitor (EIRM) that is capable of measuring outdoor ^{222}Rn concentrations accurately. The monitors used to measure the outdoor and indoor ^{222}Rn concentrations in co-operation with various laboratories and institutes in the Tokai districts[56,57] and in Japan and China[58,59,60]. In this chapter, the results of surveys in Japan and China are described.

3.2 Instruments and methods

3.2.1 Electrostatic integrating ^{222}Rn monitor

Fig. 3-1 shows the EIRM (Aloka; GS-201B) which has same construction as the EIRM developed by Iida et al.[55] The EIRM has a volume of about 2.26 L. Radon-222 atoms in the EIRM are exchanged naturally by diffusion through a membrane filter positioned at the

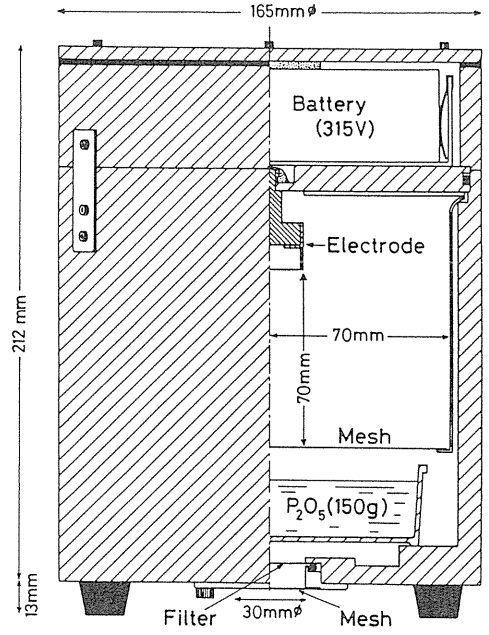

Fig. 3-1 Electrostatic integrating ^{222}Rn monitor.

bottom. The measured exchange rate was $0.67\,h^{-1}$. Radon-222 decays by emission of an α-particle to ^{218}Po, and most of ^{218}Po atoms are positively charged[61]. The positive ^{218}Po ions are collected electrostatically on the electrode. Since the electrostatic collection of $^{218}Po^{+}$ atoms depends on the humidity in air, the inside of the EIRM was dehumidified with a P_2O_5 drying agent which is powerful and does not absorb ^{222}Rn gas. The cellulose nitrate (CN) film (LR115 type 2) in the electrode detects the α-particles emitted from only ^{218}Po atoms due to the structure of the collecting electrode[55]. According to Currie's definition[62], the detection limit is found to be $0.4\,Bq\,m^{-3}$ for an exposure time of 2 months. Therefore, outdoor ^{222}Rn level can be measured with high accuracy.

3.2.2 Monitoring duration and monitor arrangement

Surveys of outdoor and indoor ^{222}Rn concentrations in the Tokai districts of Aichi, Gifu and Mie prefectures have been measured every 2 months during about 2.5 years from August 1985 to January 1988. Measurements of the outdoor ^{222}Rn concentrations at 5 locations in Japan except the Tokai districts have been carried out from December 1986 to November 1988. Surveys of indoor ^{222}Rn concentrations had also been carried out in typical dwellings in Nagoya and Sapporo from February 1984 to November 1987.

Surveys of outdoor and indoor ^{222}Rn concentrations in China have been made with about two-months integrating times from November 1988 to January 1990 and from February 1991 to March 1993. The nine central cities in six different regions of China, Changchun, Huhehaote, Beijing, Xi'an, Nanjing, Shanghai, Wuhan, Fuzhou and Guiyang, were selected as surveyed locations. Gaoxiong in Taiwan and Nagoya in Japan were selected as control cities. The first survey involved 102 measuring sites located in Beijing, Xi'an,

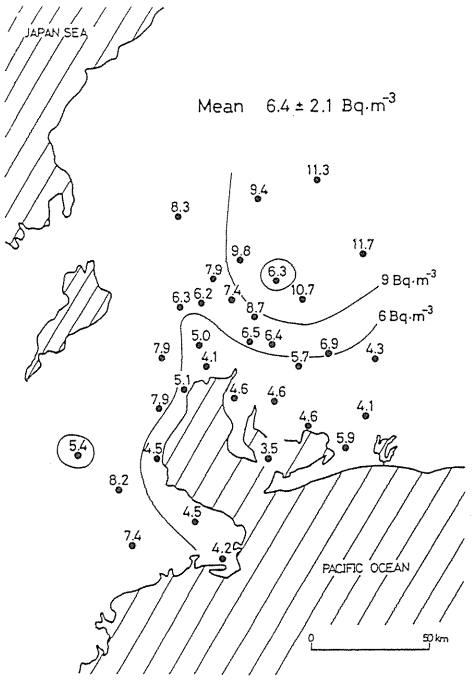

Fig. 3-2 Average outdoor ^{222}Rn concentrations at various locations in Tokai districts.

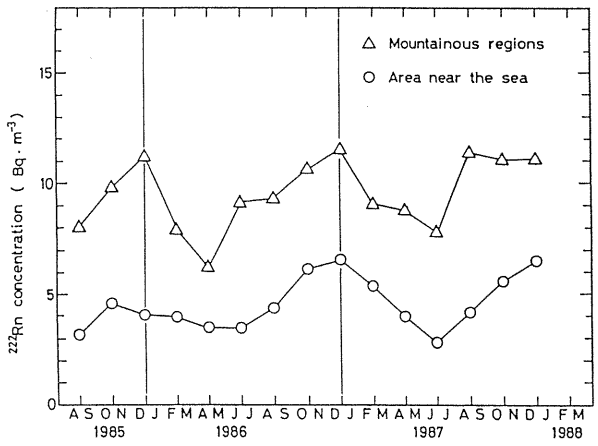

Fig. 3-3 Seasonal variation of outdoor ^{222}Rn concentrations in mountainous regions and near sea.

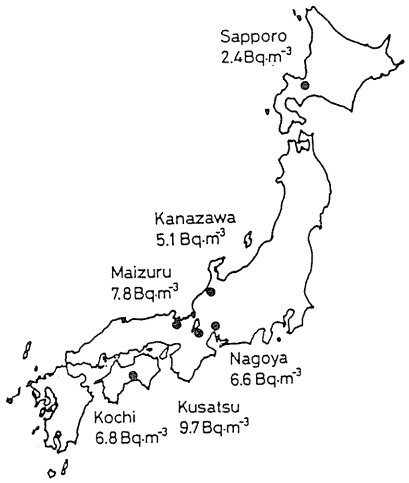

Fig. 3-4 Average outdoor ^{222}Rn concentrations at 6 locations in Japan.

Nanjing, Shanghai, Fuzhou and Guiyang and the second survey included 81 sites in Changchun, Huhehaote, Shanghai Wuhan, Fuzhou and Guiyang. In principle, the surveys were carried out by setting the monitors in indoor and outdoor conditions simultaneously at each site. The EIRMs were set outdoors ranging from 1 to 1.5 m high above the ground. The indoor monitors were set in apartments and offices constructed with concrete and brick, which are typical buildings in China.

3.3 A survey of outdoor and indoor ^{222}Rn concentrations in Japan

3.3.1 Distribution of outdoor ^{222}Rn concentrations

The annual mean ^{222}Rn concentrations at each location in the Tokai districts from August 1985 to January 1988 are shown in Fig. 3-2. The ^{222}Rn concentration at Nakatsugawa was 11.7 Bq m^{-3} which was the highest of all measured locations. On the other hand, the lowest concentration of 3.5 Bq m^{-3} was observed at Saku island. The average values of 21 locations in Aichi prefecture, 10 locations in Gifu prefecture and 9 locations in Mie prefecture were 5.7, 8.4 and 6.0 Bq m^{-3}, respectively. Fig. 3-3 compares seasonal variation of average ^{222}Rn concentrations of 8 locations in mountainous region with that of 10 locations near the sea. In the mountainous regions, the mean ^{222}Rn concentration was about 9.5 Bq m^{-3} and fluctuated widely between 6 and 11 Bq m^{-3}. On the contrary, it was 4.5 Bq m^{-3} and ranged from 3 to 6 Bq m^{-3} near the sea. The both results show a clear pattern of a spring-to-summer minimum and an autumn-to-winter maximum.

The annual mean outdoor ^{222}Rn concentrations at 5 locations in Japan except the Tokai districts are shown in Fig. 3-4. The highest concentration of 9.7 Bq m^{-3} was observed at Kusatsu and the lowest concentration of 2.4 Bq m^{-3} at Sapporo. The annual mean ^{222}Rn concentrations at Kanazawa, Maizuru and Kochi were 5.1, 7.8 and 6.0 Bq m^{-3} which were almost the same as the ^{222}Rn concentration level at Nagoya. Outdoor ^{222}Rn concentrations at Sapporo and Kanazawa did not show the clear seasonal variations. The results at other locations show a seasonal variation of a summer minimum and a winter maximum.

Table 3-1 Average outdoor and indoor ^{222}Rn concentrations in Japan.

location	average ^{222}Rn concentration (Bq m^{-3})					
	outdoor		indoor			
	No. of monitors	mean	No. of monitors	Type of house	mean	indoor / outdoor
Nagoya[a)]	1	5.9	3	wood	7.5	1.3
			5	concrete	17.7	3.0
Sapporo[b)]	1	2.2	1	wood	38.5	17.5
			2	concrete	86.1	39.1
Sapporo[c)]	1	2.3	1	wood	15.5	6.7
			2	concrete	25.2	11.0
Tokai Districts[d)]	20	5.7	13	wood	15.2	2.7
			(12	wood	11.1	1.9)[e)]
			7	concrete	13.7	2.2
mean	20	5.7	20		14.7	2.6
	(19				12.1	2.1)[e)]

a) means for Feb., 1984 ~ Jan., 1986
b) means for Feb., 1985 ~ Mar., 1986
c) means for Apr., 1986 ~ Nov., 1987
d) means for Dec., 1985 ~ Mar., 1987
e) except the data of the high ^{222}Rn concentration of 64.8 Bq m^{-3} in a wooden house.

3.3.2 Indoor ^{222}Rn concentrations

A preliminary survey of indoor ^{222}Rn concentrations had been carried out in Nagoya and Sapporo. The measurements in colder Sapporo from February 1985 to March 1986 were selected new types of energy-efficient houses which have spread gradually in Sapporo in recent years. Moreover, from April 1986 to November 1987 we have measured the ^{222}Rn concentrations in typical dwellings in Sapporo. The observed results of indoor ^{222}Rn concentrations are represented in Table 3-1. The mean ^{222}Rn concentration in 3 wooden houses at Nagoya was 7.5 Bq m^{-3} and slightly higher than the outdoor concentration of 5.9 Bq m^{-3}. The mean

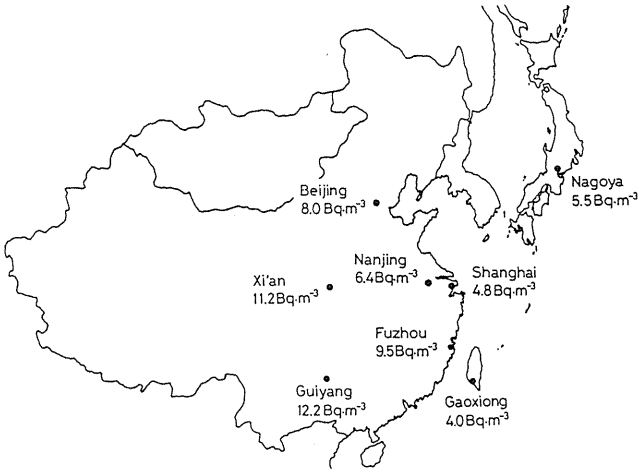

Fig. 3-5(a) Average outdoor ^{222}Rn concentrations at six cities in China from November 1988 to November 1989.

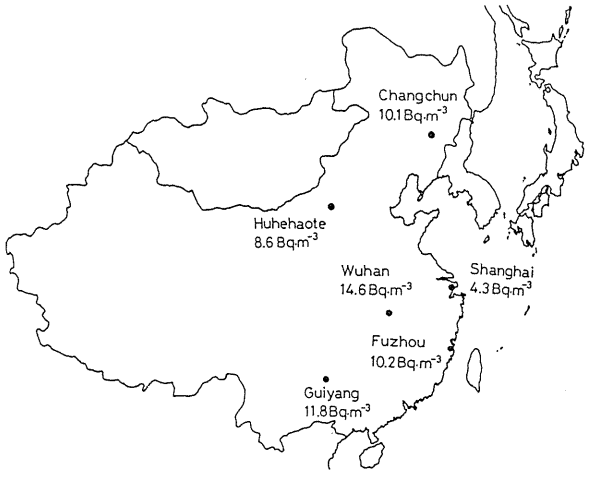

Fig. 3-5(b) Average outdoor ^{222}Rn concentrations at six cities in China from April 1991 to April 1992.

Table 3-2 Average outdoor and indoor ^{222}Rn concentrations in China (Nov., 1988 ~ Nov., 1989).

location	average ^{222}Rn concentration (Bq m^{-3})						
	outdoor			indoor			
	No. of monitors	mean	S.D.	No. of monitors	mean	S.D.	indoor / outdoor
Beijing	10	8.0	2.5	11	22.6	3.4	2.8
Xi'an	14	11.2	3.0	9	23.9	7.7	2.1
Nanjing	10	6.4	1.3	10	13.7	5.3	2.1
Shanghai	5	4.8	1.6	5	16.6	4.8	3.4
Fuzhou	10	9.5	1.9	10	24.5	5.2	2.6
Guiyang	4	12.2	2.0	4	38.1	13.9	3.1
mean		8.7	2.8		23.2	7.7	2.7
Gaoxiong[a)]	1	4.0		1	15.5	9.1	3.9
Nagoya[b)]	6	5.5		6	11.3	2.3	2.1

S.D.: standard deviation
a) means for Feb. 1988 to Feb. 1989.
b) means for Dec. 1985 to Dec. 1986.

Table 3-3 Average outdoor and indoor ^{222}Rn concentrations in China (Apr., 1991 ~ Apr., 1992).

location	average ^{222}Rn concentration (Bq m^{-3})						
	outdoor			indoor			
	No. of monitors	mean	S.D.	No. of monitors	mean	S.D.	indoor / outdoor
Changchun	7	10.1	2.0	4	26.4	4.9	2.6
Huhehaote	4	8.6	1.9	4	11.3	2.0	1.3
Shanghai	9	4.3	0.8	7	15.2	3.2	3.5
Wuhan	11	14.6	5.9	15	19.8	4.9	1.4
Fuzhou	9	10.2	2.8	9	31.8	6.5	3.1
Guiyang	1	11.8	1.1	1	17.3	6.3	1.5
mean		9.9	3.4		20.3	6.9	2.1

S.D.: standard deviation

^{222}Rn concentration in 5 concrete houses was 17.7 Bq m^{-3}, which are about 3 times those in outdoor air. The very high ^{222}Rn concentrations were observed in tightly built houses at Sapporo. On the other hand, the mean ^{222}Rn concentrations in typical dwellings at Sapporo were only about 2 times those at Nagoya.

Outdoor and indoor ^{222}Rn concentrations in 20 locations in the Tokai districts have been measured from December 1985 to March 1986 by the co-operation with NIRS[56)]. The results of annual mean ^{222}Rn concentrations in outdoor and indoor air are represented in Table 3-1. We selected 13 wooden houses and 7 concrete apartment houses. The very high ^{222}Rn concentration of 64.8 Bq m^{-3} was observed in one of wooden houses. The annual mean ^{222}Rn concentrations except the high ^{222}Rn concentration are also represented in Table 3-1. The

ratios of indoor and outdoor ^{222}Rn concentrations were 1.9 in wooden houses, 2.2 in concrete houses and 2.1 in all dwellings.

3.4 A survey of outdoor and indoor ^{222}Rn concentrations in China

3.4.1 Distribution of outdoor ^{222}Rn concentrations in China

The average outdoor ^{222}Rn concentrations at nine cities of the mainland China from November 1988 to November 1989 and from April 1991 to April 1992 are shown in Table 3-2, Table 3-3 and Fig. 3-5. Shanghai, Fuzhou and Guiyang participated in the both surveys. Their results of first and second surveys agreed fairly well for outdoor ^{222}Rn concentrations at the three cities and for indoor concentrations at Shanghai and Fuzhou. However, a different result was obtained for indoor ^{222}Rn concentrations at Guiyang, since the selected building was only one at second survey.

The annual mean ^{222}Rn concentration of nine cities was 9.3 Bq m^{-3} from Table 3-2 and Table 3-3. This is almost the same level as the average concentration of 10 Bq m^{-3} in continental areas that is indicated in UNSCEAR report[63]. Among the nine cities, the highest

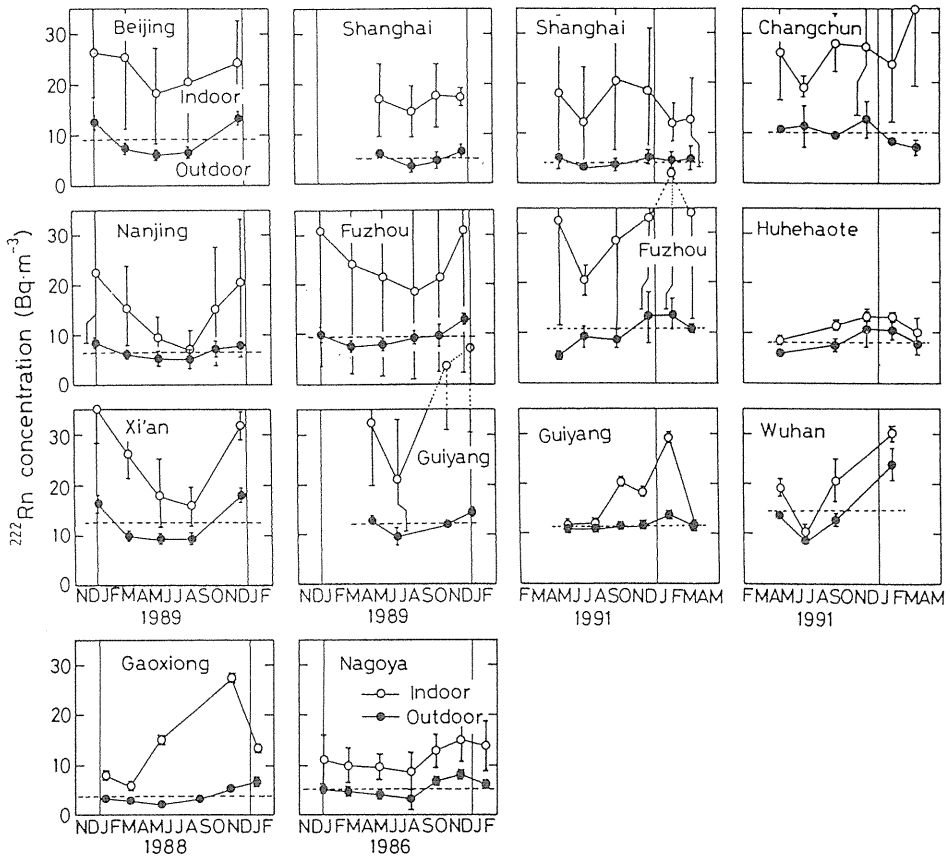

Fig. 3-6 Seasonal variation of outdoor and indoor ^{222}Rn concentrations at nine cities in China and Gaoxiong and Nagoya. The error bars indicate the standard deviations each data.

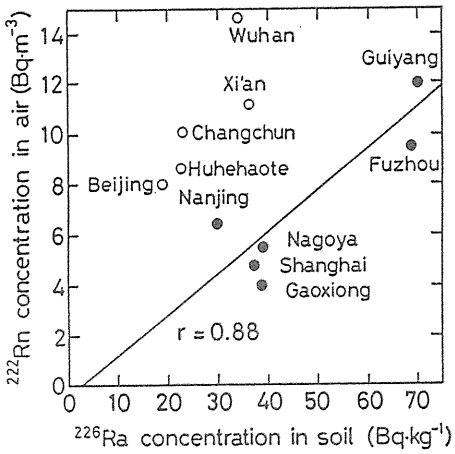

Fig. 3-7 Relationship between outdoor ^{222}Rn concentrations and ^{226}Ra concentrations in soil. A good correlation coefficient of 0.88 was obtained except for the data at Changchun, Huhehaote, Beijing, Xi'an and Wuhan.

and lowest annual mean ^{222}Rn concentrations of 14.6 Bq m^{-3} ranging from 8.4 to 23.9 Bq m^{-3} and 4.8 Bq m^{-3} ranging from 3.6 to 6.3 Bq m^{-3} were observed at Wuhan and Shanghai. The ^{222}Rn concentrations in China were higher in southern parts than those in northern parts, and they were lower in seashore are as than those in inland areas.

The mean outdoor ^{222}Rn concentrations for two-month intervals at each city are shown in Fig. 3-6. The patterns of seasonal variations at the nine cities have a summer minimum and a winter maximum, and were similar to those at control cities and most areas in the world.

Fig. 3-7 shows the relationship between outdoor ^{222}Rn concentrations and ^{226}Ra concentrations in soil[64]. A good correlation coefficient of 0.88 was obtained for the data at Nanjing, Shanghai, Fuzhou, Guiyang, Nagoya and Gaoxiong. The data at Changchun, Huhehaote, Beijing, Xi'an and Wuhan were excluded from the calculation of the correlation coefficient, because of the reasons described below. The high outdoor ^{222}Rn levels at Changchun, Huhehaote, Beijing and Xi'an suggest the high exhalation rate of ^{222}Rn from dry soil of low ^{226}Ra concentrations. In addition, some of the high ^{222}Rn concentrations may be attributed to high atmospheric stability and high frequent occurrence of inversions in the inland areas. The low ^{222}Rn levels at Nanjing and Shanghai correspond to the low exhalation rate of ^{222}Rn from soil due to the low ^{226}Ra concentrations in soil and high soil moisture. The high ^{222}Rn levels at Fuzhou and Guiyang result mainly from the high ^{226}Ra concentrations in soil. A clear seasonal variation at Wuhan situated in inland area may be caused by high atmospheric stability and low soil moisture in winter.

3.4.2 Indoor ^{222}Rn concentrations

Annual means and seasonal variations of indoor ^{222}Rn concentrations were also shown in Table 3-2, Table 3-3 and Fig. 3-6. The highest mean concentration of 38.1 Bq m^{-3} was observed at Guiyang in the first survey, and the lowest was 11.3 Bq m^{-3} at Huhehaote. The seasonal pattern of the indoor ^{222}Rn concentrations was the same as that of outdoor, i.e., that was minimum in summer and maximum in winter. This trend depends upon not only outdoor ^{222}Rn concentrations but also living conditions, being ventilated in summer. As shown in the

right column of Table 3-2 and Table 3-3, the ratios of indoor to outdoor ^{222}Rn concentrations in China ranged from 1.3 to 3.4, were really same as those of Japan[60].

3.5 Conclusion

Outdoor and indoor ^{222}Rn concentrations have been surveyed in the Tokai districts and in Japan and China using passive electrostatic integrating ^{222}Rn monitors.

In the Tokai districts of Aichi, Gifu and Mie prefectures, outdoor ^{222}Rn concentrations have been measured at 40 locations every 2 months during about 2.5 years from August 1985. The annual mean ^{222}Rn concentrations were about 9.5 and 4.5 Bq m^{-3} in the mountainous regions and near the sea. The both bimestrial results show clear seasonal variations. The annual mean outdoor ^{222}Rn concentrations at Sapporo, Kanazawa, Maizuru, Nagoya, Kusatsu and Kochi were 2.4, 5.1, 7.8, 6.6, 9.7 and 6.8 Bq m^{-3}, respectively. Outdoor ^{222}Rn concentrations showed different seasonal patterns at 6 locations. The average indoor ^{222}Rn concentrations in wooden and concrete houses were about 11.1 and 13.7 Bq m^{-3} in the Tokai districts. The ratio of mean indoor and outdoor ^{222}Rn concentrations of 12.1 and 5.7 Bq m^{-3} were about 2.1 in the dwellings.

The surveys of outdoor and indoor ^{222}Rn concentrations at nine cities in China were been carried out by the co-operation of China and Japan from November 1988 to January 1990 and February 1991 to March 1993. In the first survey, the annual mean outdoor ^{222}Rn concentrations at Beijing, Xi'an, Nanjing, Shanghai, Fuzhou and Guiyang were 8.0, 11.2, 6.4, 4.8, 9.5 and 12.2 Bq m^{-3}, respectively. The results of the second survey at Changchun, Huhehaote, Shanghai, Wuhan, Fuzhou and Guiyang were 10.1, 8.6, 4.3, 14.6, 10.2 and 11.8 Bq m^{-3}, respectively. The annual mean ^{222}Rn level and seasonal variation at each city can be explained by the ^{226}Ra concentrations in soil, the weather conditions, the soil moisture and their geological conditions. The annual mean indoor ^{222}Rn concentration was 21.8 Bq m^{-3} in typical buildings constructed with concrete and brick. The highest indoor ^{222}Rn concentration of 38.1 Bq m^{-3} was observed at Guiyang, and the lowest concentration of 11.3 Bq m^{-3} was at Huhehaote. The seasonal variations of the ^{222}Rn concentrations in the dwellings depend upon outdoor ^{222}Rn concentrations and living conditions. The ratios of indoor to outdoor ^{222}Rn concentrations ranged from 1.3 to 3.4.

4. Continuous Measurements of Outdoor Radon Concentrations at Various Locations in East Asia

4.1 Introduction

To investigate ^{222}Rn behavior in the atmosphere, continuous ^{222}Rn monitors, which can measure outdoor ^{222}Rn concentrations accurately at numerous locations, are required. Ionization chamber[65], scintillation cell[66], the two-filter method[67], and electrostatic collection method[68] have been used for measuring environmental ^{222}Rn concentrations. However, these instruments and methods reported up to the present were not suitable to measure outdoor low ^{222}Rn concentrations. Authors[69] studied and developed an electrostatic continuous ^{222}Rn monitor (ERM-1). This ^{222}Rn monitor has following characteristics: 1) a capability to measure continuously low ^{222}Rn concentration levels with high accuracy and sensitivity; 2) a stable operation; and 3) an easy maintenance. Using this monitor, outdoor ^{222}Rn concentrations were measured at Nagoya University beginning in 1985.

This chapter describes the construction and characteristics of four ^{222}Rn monitors (ERM-3, ERM-4, ERM-5, and ERM-6) which were the same type as ERM-1 and some results for the continuous measurements.

4.2 Measurement method

4.2.1 Construction and principle of electrostatic ^{222}Rn monitor

Fig. 4-1 shows the schematic diagram of the monitor. The ^{222}Rn detection unit is equipped in the center of an aluminum hemisphere with radius 200 mm. The monitor has a volume of about 16.8 L. The air flows at 1 L min^{-1} into the hemisphere through a membrane filter and a vapor trap of phosphorus pentoxide (P_2O_2) with a diaphragm pump. This process removed aerosols, ^{222}Rn daughters and water vapor from the air.

Radon-222 decays by emission of an α-particle to ^{218}Po, and most of ^{218}Po atoms are positively charged[70]. The positive ^{218}Po ions are collected electrostatically on the electrode of aluminized Mylar (0.9 mg cm^{-2}) coated with 10 mg cm^{-2} ZnS(Ag) phosphor[71]. Alpha-particles emitted from ^{218}Po and ^{214}Po atoms are incident on the underlying ZnS(Ag) through the Al Mylar. The scintillations due to α-particles are detected by a 38 mm diameter photomultiplier tube optically coupled to a light pipe. The scintillation pulse which is amplified and processed is fed into a personal computer (NEC PC-9801RX) through an interface. In the personal computer, the ^{222}Rn concentrations are calculated automatically from α-counts accumulated every one-hour using following equation,

$$Q(I) = \frac{C(I) - \sum_{i=1}^{5} C'(I-i)}{CF \cdot F(I)} \tag{4-1}$$

where, Q(I) is the mean ^{222}Rn concentration during the time interval I in Bq m^{-3}; C(I) is the α-counts during time interval I; C'(I-i) is the α-counts during time interval I that are expected from ^{222}Rn daughters collecting on the electrode during time interval I-i; CF is a calibration factor given by the product of η_{Po}, η_{ZnS} and V which are the collection efficiency of $^{218}Po^+$ ions on the electrode, the α-counting efficiency by the ZnS(Ag) phosphor and the volume of the hemisphere in m 3; and F(I) is a term on the basis of Bateman equation in s. The term F(I) is a function of the decay rates of ^{222}Rn daughters, the collecting time of $^{218}Po^+$ ions on the electrode and the α-counting time[72].

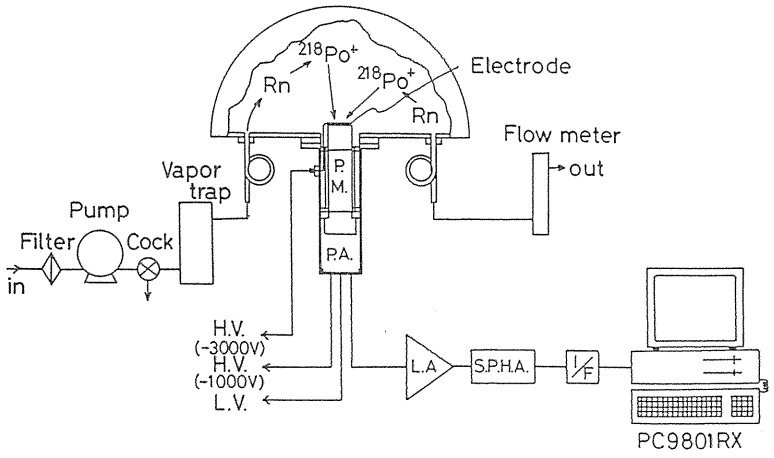

Fig. 4-1 Schematic diagram of continuous electrostatic ^{222}Rn monitor.

4.2.2 Characteristics of the ^{222}Rn monitors

A flow rate sucked with the diaphragm pump was adjusted to 1 L min^{-1}, in consideration of the exchange rate in the ^{222}Rn monitor, the presence of ^{220}Rn in the sampling air, and the amount of drying agent in the vapor trap. Up to the flow rate of 0.5 L min^{-1}, the ^{222}Rn concentration in the monitor varies almost identically that in outdoor environment.

The electric field inside the monitor was calculated using a computer simulation. From the lines of electric force, the effective collection volume from which $^{218}Po^{+}$ ions could be collected on the electrode can be evaluated to be almost the whole volume.

The electrostatic collection of $^{218}Po^{+}$ ions depends on the humidity in the air[70]. In practice, it was confirmed experimentally that the collection efficiency of $^{218}Po^{+}$ ions decreases with increasing absolute humidity. The relative or absolute humidity in the outdoor environment fluctuates considerably from season to season. Therefore, the air sample was passed through a vapor trap of about 1000 g of P_2O_5 which could maintain the inside of the monitor at absolute humidity under 0.5 g m^{-3} during a hot and humid summer in Japan and China.

The $^{218}Po^{+}$ ions may also be neutralized by trace gases[73], especially NO_2. The calibration factor CF at an applied potential of −3000 V as a function of NO_2 vapor concentration indicated that it did not change within the NO_2 concentration range of 0 to 0.53 mg m^{-3} at 25°C, 1 atm. Because the collection efficiency of the $^{218}Po^{+}$ ions was not affected by the neutralization due to NO_2, no attempt was made to remove NO_2.

The dependence of the calibration factor CF upon the applied potential was measured from −500 V to −5000 V in steps of 500 V, keeping the absolute humidity under 0.5 g m^{-3}. The experimental result showed that the calibration factor increased only 18% from −2000 V to −5000 V. Therefore, the applied potential has been determined to be −3000 V, reducing the various effects due to electric leakage.

Calibrations of five ^{222}Rn monitors including ERM-1 were done as follows: the five monitors, 108.7 L vessel, a 1.5 L cylindrical ionization chamber containing high ^{222}Rn concentration, a vapor trap of P_2O_5 and a diaphragm pump were connected in series in a recirculating system. Then, the air was circulated for 24 hours at 1 L min^{-1} through the system with the pump. The ^{222}Rn concentration in the system was measured with the 1.5 L ionization chamber that had been calibrated against known concentration of ^{222}Rn exhaled from ^{226}Ra solution. The mean values of the calibration factors are 17.8, 18.6, 18.3, 18.1 and 19.3 $Bq^{-1}\,m^3\,h^{-1}$ for ERM-1, ERM-3, ERM-4, ERM-5 and ERM-6, respectively. The product of the collection efficiency η_{Po} and the α-counting efficiency η_{ZnS} can be evaluated to be about 0.3 from the CF values. Assuming that η_{ZnS} is 0.45 and 88% of ^{218}Po atoms carries a positive charge when formed[73], about 75% of the $^{218}Po^{+}$ ions in the monitor were collected on the electrode.

To study the effect of the recombination between $^{218}Po^{+}$ ions and negative ions in high ^{222}Rn concentration, the relationship between the calibration factor and the ^{222}Rn concentration was measured. This measurement was carried out using ERM-1. The relationship was linear in the range from 18 to 2220 Bq m^{-3}.

The background count rate of each ^{222}Rn monitor was measured for 24 hours by maintaining ^{222}Rn-free in the monitors after flowing 100 L of ^{222}Rn-free air that is a mixture of nitrogen and oxygen in the ratio of 79 to 21 in volume. The mean background count rates obtained from this experiment are $(5.3 \pm 2.7)\,h^{-1}$. Using the values of the uncertainty in the background count rates and the calibration factors, the detection limits defined by Currie[74] were found to be about 0.3 Bq m^{-3} for every monitor.

When the ^{222}Rn concentrations were measured continuously at one-hour intervals with the monitor, the standard deviations could be evaluated by using the statistical errors of α-counts and by considering propagation of the errors in Eq. 4-1. The calculations gave the standard deviations of 23.7, 10.6 and 7.5% for the ^{222}Rn concentrations of 1, 5 and

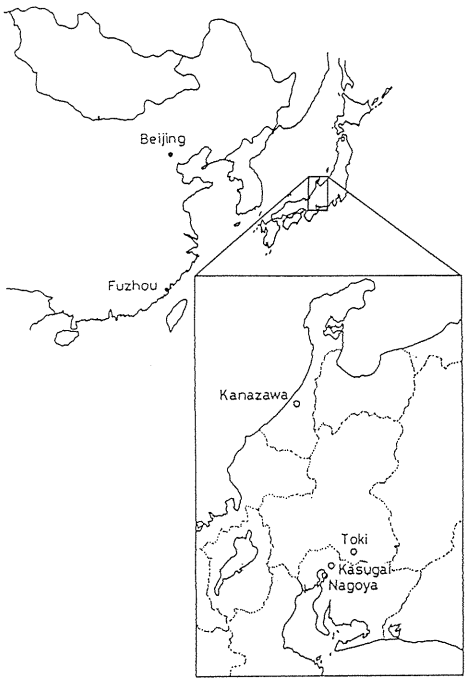

Fig. 4-2 Map of ^{222}Rn measurement locations.

10 Bq m^{-3}, respectively. Since the standard deviations of monthly and annual mean ^{222}Rn concentrations due to the statistical errors of α-counts were small, the uncertainty of the mean concentrations depended mainly on the uncertainty of the calibration factor and accidental noise counts.

The maintenance of the ^{222}Rn monitor was only to exchange the filter paper and the drying agent of P_2O_5 once a month. Since ^{222}Rn long-lived decay products of ^{210}Pb accumulate on the Al Mylar of the electrode for long-term measurements, it was necessary to remeasure the background count rate or to exchange the Al Mylar + ZnS(Ag) sheet once a year. The data of ^{222}Rn concentrations were stored in a floppy disk at 12 p.m. every day.

4.3 Results and discussion

4.3.1 Outdoor ^{222}Rn concentrations in Japan

After studying the characteristics of the monitors, outdoor ^{222}Rn concentrations were continuously monitored beginning in October 1990 at Kasugai (ERM-6) in the plains, Toki (ERM-4) in the mountainous regions, and Kanazawa (ERM-5) located near the Japan Sea. The monitors were set up at typical locations in these regions. The locations are shown in Fig. 4-2. The distances from Nagoya to Kasugai, Toki and Kanazawa are about 10 km, 30 km and 150 km, respectively. The hourly data of ^{222}Rn concentrations were obtained from August 1985 to August 1994 at Nagoya, from October 1990 to September 1993 at Kasugai, from October 1990 to April 1992 at Toki and from November 1990 to October 1994 at Kanazawa.

Fig. 4-3 shows the typical diurnal variations of ^{222}Rn concentrations in each season of 1991 at each location. The ^{222}Rn concentrations from 1 to 10 January, shown in Fig. 4-3(a), illustrated similar variation at each location. The ^{222}Rn concentrations during 3 and 7 January hardly fluctuated and were low. Most of the low concentrations of about 3 Bq m^{-3} are regarded as the contribution from the ^{222}Rn originating in China[75], since Japan was then covered with a cold air mass from the continent and the strong northwest wind was blowing. The results from 21 to 30 April, shown in Fig. 4-3(b), were low ^{222}Rn concentration levels at

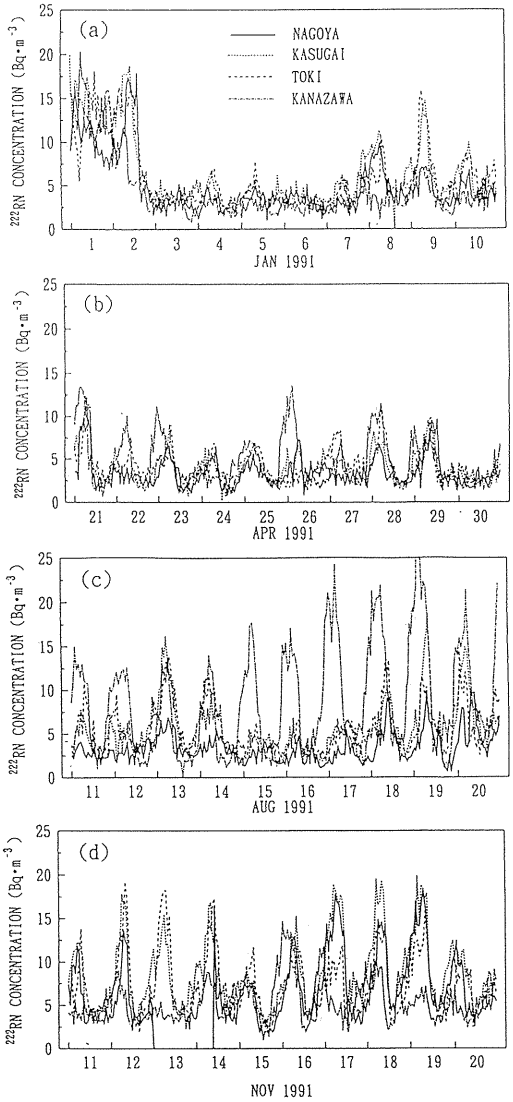

Fig. 4-3 Comparison of ^{222}Rn concentrations measured at Nagoya, Kasugai, Toki and Kanazawa from (a) 1 to 10 January, 1991, (b) 21 to 30 April, 1991, (c) 11 to 20 August, 1991 and (d) 11 to 20 November, 1991.

every location. The ^{222}Rn concentrations at Kasugai and Toki indicated hourly variations similar to Nagoya. The hourly variations of ^{222}Rn at Kanazawa were a little different from other locations. The ^{222}Rn concentrations at Kasugai and Toki from 11 to 20 August, shown in Fig. 4-3(c), were a little higher than those at Nagoya. Since a south wind blows mainly in summer, the ^{222}Rn concentrations at Nagoya located near the seacoast showed a small

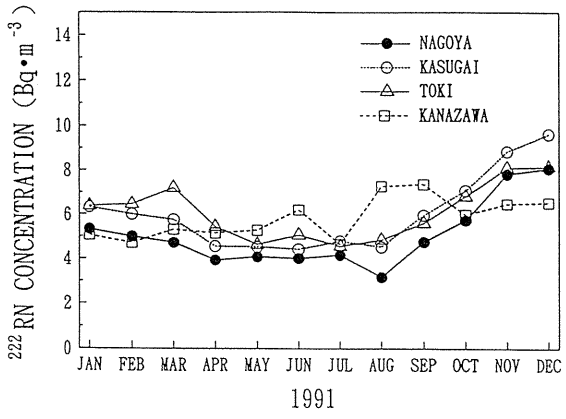

Fig. 4-4 Seasonal variation of monthly mean ^{222}Rn concentrations at Nagoya, Kasugai, Toki and Kanazawa.

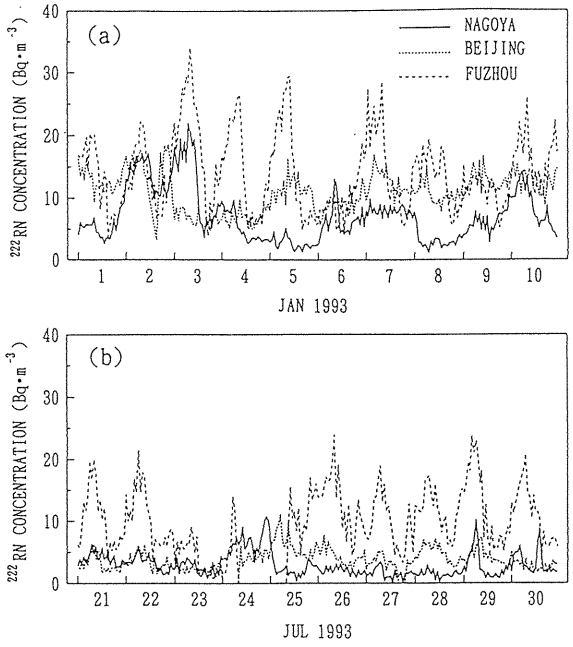

Fig. 4-5 Comparison of ^{222}Rn concentrations measured at Nagoya, Beijing, and Fuzhou from (a) 1 to 10 January, 1993 and (b) 21 to 30 July, 1993.

diurnal variation and the mean level was low. On the other hand, the ^{222}Rn concentrations at Kanazawa showed large and clear diurnal variations that may be attributed to strong inversion conditions. The clear diurnal variations at Nagoya, Kasugai and Toki from 11 to 20 November are shown in Fig. 4-3(d). The diurnal variation at Kanazawa is not clear and the mean ^{222}Rn level was low.

The mean ^{222}Rn concentrations each month were calculated using the hourly data to investigate the seasonal variations of the ^{222}Rn concentrations at each location. The seasonal variations in 1991 are shown in Fig. 4-4. The annual mean ^{222}Rn concentrations at Nagoya, Kasugai, Toki and Kanazawa were 5.1, 6.0, 6.1 and 5.8 Bq m^{-3}, respectively. The ^{222}Rn level at Kasugai was a little higher than that at Nagoya. However, the seasonal variations of a spring-summer minimum and an autumn-winter maximum were similar to that at Nagoya. The seasonal pattern at Toki was similar to that at Nagoya except for a higher ^{222}Rn level in March. On the other hand, the monthly mean ^{222}Rn concentration at Kanazawa showed a different seasonal pattern with a summer-autumn maximum. As described above, the high mean ^{222}Rn concentrations were observed in August and September. Similar annual mean ^{222}Rn concentrations and the seasonal pattern at each location had already been observed by passive method[76].

4.3.2 Outdoor ^{222}Rn concentrations in China

After comparison of the two ^{222}Rn monitors of ERM-1 and ERM-3 in the campus of Nagoya University, the ERM-3 was sent to Fuzhou, China and outdoor ^{222}Rn concentrations were measured beginning in July 1991. ERM-4 was moved from Toki to Beijing, China. The outdoor ^{222}Rn concentrations at Beijing were measured for September 1992 to September 1993. The locations are shown in Fig. 4-2.

Fig. 4-5 shows the typical diurnal variations of ^{222}Rn concentrations in January and July 1993 at Nagoya, Beijing and Fuzhou. In Fig. 4-5, the hourly data are plotted at each local time, and the results at Nagoya, Beijing and Fuzhou are shown by solid lines, broken lines and dotted lines, respectively. Both ^{222}Rn concentrations from 1 to 10 January and from 21 to 30 July showed different diurnal variation at each location. From the figures, it is clear that the mean ^{222}Rn levels at Fuzhou were higher than those at Nagoya and Beijing. These tendencies appeared in all seasons.

The monthly mean ^{222}Rn concentrations were calculated using the hourly data from October 1992 to September 1993. The data obtained at Fuzhou were of poor quality because of

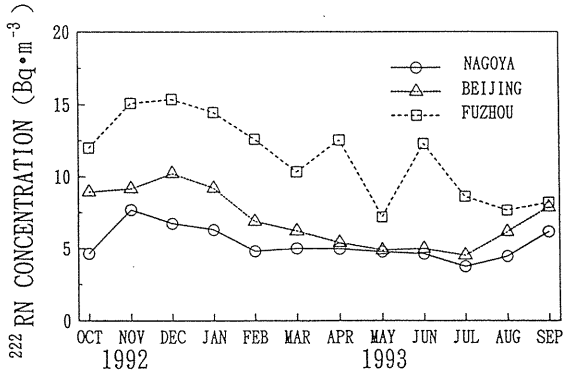

Fig. 4-6 Seasonal variation of monthly mean ^{222}Rn concentrations at Nagoya, Beijing and Fuzhou.

an electric power shortage in that area, especially during summer. The variations are shown in Fig. 4-6. The mean ^{222}Rn concentrations during this period at Nagoya, Beijing and Fuzhou were 5.3, 7.0 and 11.4 Bq m^{-3}, respectively. The monthly mean ^{222}Rn level at Fuzhou was high. However, the seasonal variation of a summer minimum and a winter maximum was similar at each location. The annual mean outdoor ^{222}Rn concentrations at Beijing and Fuzhou[77] measured with passive monitors were 8.0 and 9.5 Bq m^{-3}. Therefore, the ^{222}Rn concentrations observed with electrostatic ^{222}Rn monitor are consistent with the results by passive method.

4.4 Conclusions

Four electrostatic ^{222}Rn monitors were constructed for continuously measuring outdoor ^{222}Rn concentrations at various locations. The characteristics of the monitors were studied in detail.

The hourly data of outdoor ^{222}Rn concentrations were obtained at Nagoya, Kasugai, Toki and Kanazawa in Japan, and Beijing and Fuzhou in China. The ^{222}Rn concentrations at Nagoya, Kasugai and Toki showed a diurnal variation clearly in autumn and a seasonal pattern of a spring-summer minimum and an autumn-winter maximum. At Kanazawa, a diurnal variation appears clearly in summer. At Beijing and Fuzhou, the pattern of the diurnal variations was different from that at Nagoya. The annual mean ^{222}Rn concentrations at Nagoya, Kasugai, Toki, and Kanazawa in Japan, and at Beijing and Fuzhou in China were 5.1, 6.0, 6.1, 5.8, 7.0, and 11.4 Bq m^{-3}, respectively.

5. A Long Range Transport Model and Simulation Study on the Temporal Variation of Radon

5.1 Introduction

Many researchers have studied the diurnal variations and the vertical profiles of ^{222}Rn mainly based on the stability of the air, eddy diffusivity, and the diffusion equation. However, until now the analyses about the seasonal variation and long range transport of ^{222}Rn are very limited[78,79]. In addition, numerical simulation studies about the observed temporal variation of ^{222}Rn are also limited[80]. In this chapter, first we propose an analytical treatment of long range transport of ^{222}Rn with an aim to clarify origin and transport of ^{222}Rn. Next we intend to develop the numerical model of three dimensional transport of ^{222}Rn from remote and near sources. This model should be applied to the transport of various pollutant gases. ^{222}Rn is a convenient tracer element of atmospheric transport, because it is chemically inert and a radioactive gas with the long half life time of 3.8 days. Continuous measurement of environmental ^{222}Rn concentration has been carried out in Nagoya University for this decade. In order to clarify the variation of ^{222}Rn concentration, the results of numerical simulation was compared to the observational data.

5.2 A long range transport model of ^{222}Rn

5.2.1 Analysis

Fig. 5-1 shows an example of the variation of ^{222}Rn concentration measured at Nagoya University. In this work we separate the ^{222}Rn concentration to the following two components:

(1) Rn atoms originated near the measuring site, which is denoted hereafter by "diurnal

variation component." For this component, the time variation may be controlled by factors such as atmospheric stability, eddy diffusivity, and Rn exhalation rate near the site.
(2) Rn atoms originated from remote sources, which is denoted hereafter by "background component." This component is assumed to be distributed uniformly in the atmospheric boundary layer since these Rn atoms have been mixed enough in the boundary layer until they arrive at the measuring site from their origin.

According to three-dimensional numerical simulations of atmospheric radon[81], we define here that "diurnal variation component" is consisted of radon exhaled within 20 km around measuring site, and the rest is "background component." The average minimum of the day concentration of the "diurnal variation component" was adopted to be about 0.8 Bq/m^3 [81]. In Fig. 5-1, a broken line represents background component. The curve was drawn about 0.8 Bq/m^3 below the minimum concentration on each day.

The radon concentration obtained by a filter-pack method at the campus during summer

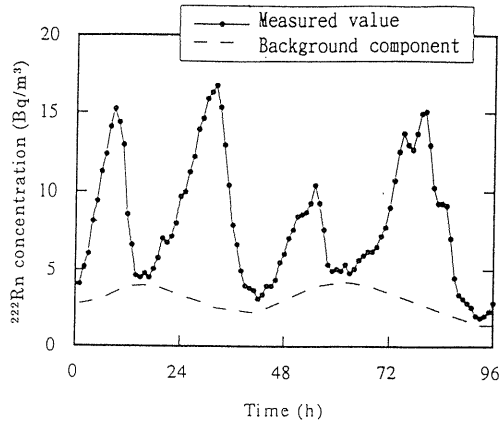

Fig. 5-1 An example of the variation of ^{222}Rn concentration.

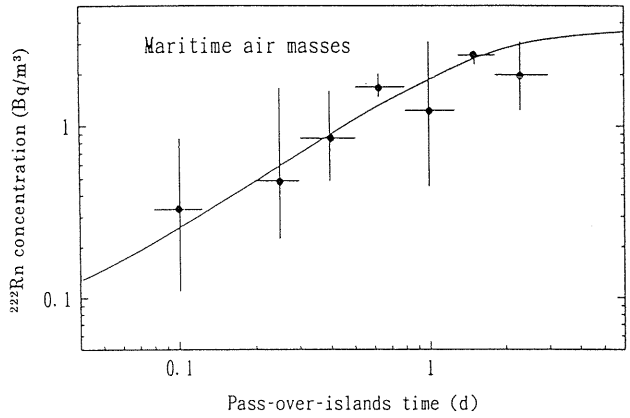

Fig. 5-2 The relation between the background component and the pass-over-island time (maritime air mass).

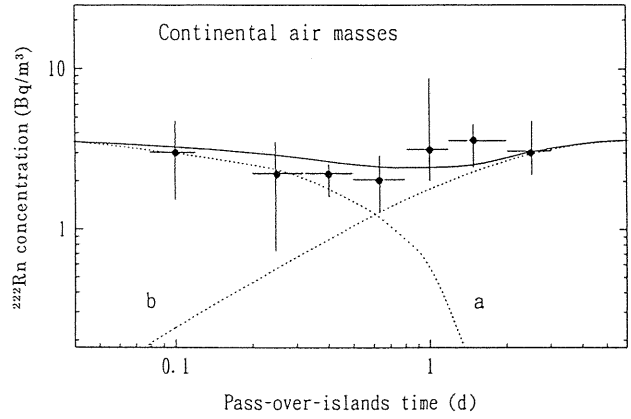

Fig. 5-3 The relation between the background component and the pass-over-island time (continental air mass).

season (July—Sept., 1977, 1978, 1981) and during winter season (Dec. 1980—March 1981) was analyzed. An air mass trajectory was drawn on each day by using 850 mb weather chart. According to the history of the air arrived at Nagoya, the observed air mass was classified into two groups ----- maritime air mass and continental air mass.

Fig. 5-2 shows the relation between the background component of Rn concentration and the pass-over-island time in the case of maritime air mass[82]. The pass-over-island time on Japan Island was determined from the trajectories described above.

Fig. 5-3 shows the relation in the case of continental air mass.

5.2.2 Model

According to the analysis described in 5.2.1, the concentration of background component Rn, n, is given by

$$\frac{dn}{dt} = -(\lambda_d + \lambda_r)n + S \tag{5-1}$$

where, t : The pass-over island time (d)
λ_r : removal constant from the atmospheric boundary layer to the upper free atmosphere (d^{-1})
λ_d : radioactive decay constant (d^{-1})
S : rate of Rn supply (Bq m^{-3} d^{-1}).

S is given by

$$S = E/H \tag{5-2}$$

where, E : Rn exhalation rate (Bq m^{-2} d^{-1})
H : height of the atmospheric boundary layer (m).

In the case of maritime airmass, we obtain the solution of eq. (1) from the initial condition : t = 0 : n = 0,

$$n = \frac{S}{\lambda}(1 - e^{-\lambda T}) \tag{5-3}$$

where $\lambda = \lambda_r + \lambda_d$ and T is the pass-over islands time from landing point in Japan Islands to Nagoya. The solid line shown in Fig. 5-2 is drawn using the values of $\lambda = 0.68d^{-1}$ from $\tau_R = 1/\lambda_R = 2$ days and $S/\lambda = 3.7\,\mathrm{Bq\,m^{-3}}$. The saturation concentration of n $(t \to \infty) = S/\lambda = 3.7\,\mathrm{Bq\,m^{-3}}$ was determined from the observed data in Fig. 5-3.

In the case of continental air mass, the solution of eq. (5-1) is shown by

$$n = \frac{S}{\lambda}(1 - e^{-\lambda T}) + \frac{S}{\lambda} e^{-\lambda(K+1)T} \tag{5-4}$$

where K=T'/T and T' is the time from leaving point of Chinese Continent to landing point of Japan Islands. The solid line in Fig. 5.3 is drawn from eq. (5-4) using the average value of K of about 1.6.

5.2.3 Discussion

In Figs. 5-2 and 5-3, the observed data agree fairly well with model curves respectively. The value of τ_R=2 days seems to be consistent with the values obtained by Misaki et al[83]. and Mochizuki and Tanji[84].

In the treatment described above, we can obtain the value S=2.5 $\mathrm{Bq\,m^{-3}\,d^{-1}}$. If we adopt the value of E=1 Rn atom $\mathrm{cm^{-2}s^{-1}}$=1.8×10^3 $\mathrm{Bq\,m^{-2}\,d^{-1}}$ [85,86] as the exhalation rate of radon over the land, we get H=720 m from eq. (5-2), which is consistent with the height of atmospheric boundary layer (0.5−1.5 km).

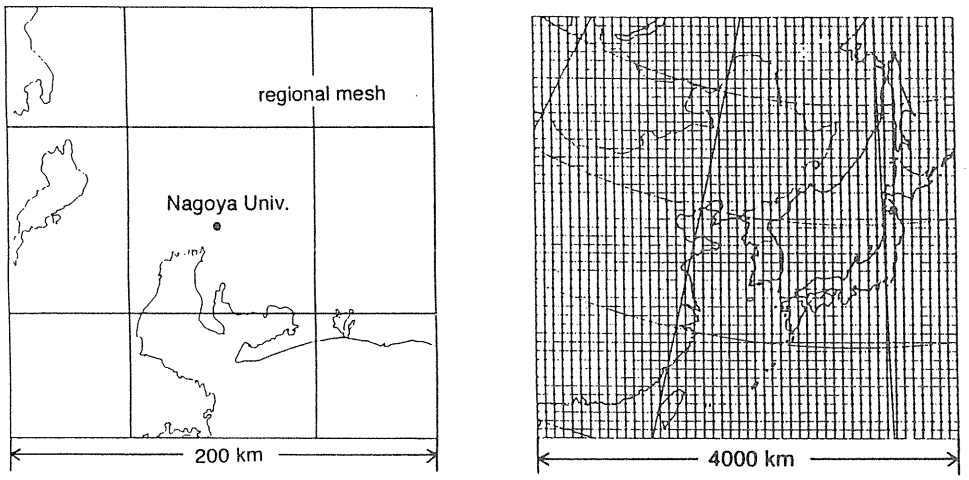

Fig. 5-4 Computational areas. (a) local area (b) regional area.

5.3 The numerical model on three dimensional atmospheric transport of ^{222}Rn

5.3.1 Modeling system

(1) Computational areas

Considering the 3.8 days half life time of ^{222}Rn, we take the computational area to be a broad region over the eastern Asia. This area is subdivided into two regions: local area (200 km×200 km) centered on Nagoya and regional area (4000 km×4000 km) which covers the large part of eastern Asia. Fig. 5-4(a) and (b) show the local and regional areas, where the horizontal grid resolutions are $\Delta x = \Delta y = 4$ *km* and $\Delta x = \Delta y = 80$ *km*, the altitude of the upper boundary are 1 *km* and 4 *km*, and the vertical grid resolutions are $\Delta z = 50$ *m* and $\Delta z = 200$ *m*, respectively. The ^{222}Rn from the local area around the measuring site dominates the diurnal variation of its concentration, while the ^{222}Rn from the regional area affects the long-time variation.

(2) Wind field model

We used the data of WMO, electric power plants at Hamaoka, and AMeDAS (Automated Meteorological Data Acquisition System), where the periods were 28 May to 18 April 1990, 1 November to 18 November 1990, and 10 December 1990 to 3 January 1991. The surface and aerological data of wind field were interpolated to fit for the calculational mesh. However, the interpolated wind field does not satisfy the equation of continuity,

$$\frac{\partial}{\partial x}\left(\frac{\rho u}{m}\right)+\frac{\partial}{\partial y}\left(\frac{\rho v}{m}\right)+\frac{1}{m^2}\frac{\partial(\rho w^*)}{\partial z^*}=0\,. \tag{5-5}$$

Here the (u, v, w) are components of wind velocity along the axes of x, y, z. The map scale factor m is the ratio of the transformed distance on the Lambert conformal map projection to the true distance, while m is equal to 1 on the local area. ρ is the density of air. z^* is the terrain following coordinate. In the regional area, z^* is equal to $(z - z_g)/(z_t - z_g) \times z_t$, while z^* is equal to z in the local area. z_g is elevation of ground. z_t is reference altitude for the upper boundary.

We modified the interpolated wind field so as to satisfy this equation with variational method (Ishikawa, 1991). The calculated wind field was provided at 6 hours resolution and linearly interpolated to the time step of the transport model.

(3) Transport model

This transport model is based on WSPEEDI, JAERI (World System for Prediction of Environmental Emergency Dose Information, Japan Atomic Energy Research Institute)[87,88].

$$\frac{\partial c}{\partial t}=-m^2\left\{\frac{\partial}{\partial x}\left(\frac{uC}{m}\right)+\frac{\partial}{\partial y}\left(\frac{vC}{m}\right)\right\}$$

$$-\frac{\partial wC}{\partial z^*}+\frac{\partial}{\partial z^*}\left(K\frac{\partial C}{\partial z^*}\right)-\lambda C+S \tag{5-6}$$

Here C is ^{222}Rn concentration (Bq m^{-3}). λ is the decay constant (2.097×10^{-6} s^{-1}) of ^{222}Rn. K is the vertical diffusion coefficient (m^2 s^{-1}). S is ^{222}Rn emission rate (Bq m^{-3} s^{-1}). m is the map scale factor. z* is the terrain following coordinate.

We used the diffusion equation of ^{222}Rn with the horizontal advection, vertical advec-

tion, vertical diffusion, radioactive decay, and emission. The equation was solved by the different techniques for the local and regional areas, respectively, shown in Table 5-1. The time steps of local and regional areas were set equal to 150 s and 300 s, respectively.

Table 5-1 Numerical Method

	Local	Regional
Advection Scheme	random-walk method	finite difference scheme Modified EXQUISITE method (Maekawa, 1987)[89]
Diffusion Scheme	random-walk method (Diehl et al., 1982)[90]	finite difference scheme Crank-Nicolson method (Smith, 1965)[91]

(4) Distribution of ^{222}Rn emission rate

The area of ^{222}Rn emission for the local area was difined as a section (80 km×80 km) centered on Nagoya. This source contributes to the results of the local calculation, while ^{222}Rn emitted in the outside of this section contribute to the results of the regional one. The flux of ^{222}Rn from the oceans was assumed zero, because oceanic emission was 100—1000 times smaller than the emission from the land areas.

The distribution of the ^{222}Rn emission rate shown in Fig. 5-5(a) was determined for the local area, assuming the following linear relation between the average ^{222}Rn concentration and ^{222}Rn emission rate[75]:

$$Q = 0.48E + 2.3 \tag{5-7}$$

where Q and E are the annual average of concentration (Bq m^{-3}) and emission rate (Bq m^{-2} s^{-1}) respectively.

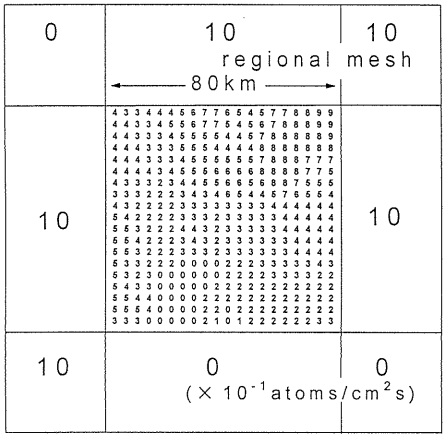

Fig. 5-5(a) Distribution of ^{222}Rn emission rate in the local area.

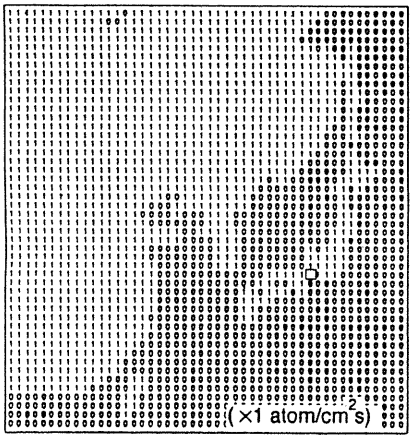

Fig. 5-5(b) Distribution of ^{222}Rn emission rate in the regional area.

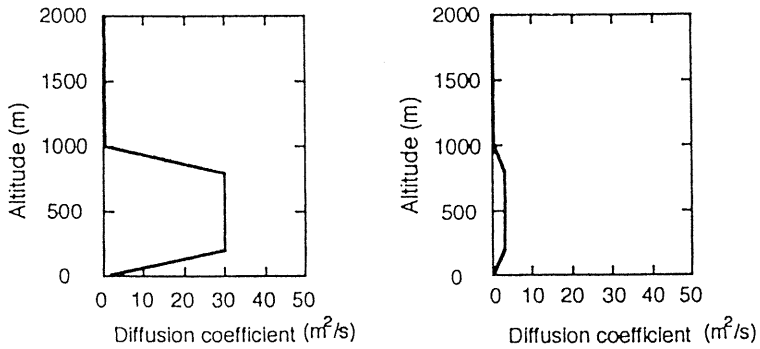

Fig. 5-6 Vertical turbulent diffusion profiles for the regional area.

Fig. 5-5(b) shows the distribution of ^{222}Rn emission rate in the regional area. We simply assumed the uniform emission rate (1 Rn atom $cm^{-2} s^{-1}$). The square represents the ^{222}Rn emission part for the local area.

(5) Vertical turbulent diffusion profiles

We used the different profiles for the local and regional areas because the detailed meteorological data were available only on the local area. The profiles of the local area were calculated by Mellor and Yamada's turbulence model[92]. For the regional area, we used simple profiles to classify the unstable (for day-time) and stable conditions (for night-time). Fig. 5-6 shows the simple profiles for the regional area.

5.3.2 Results

The results of numerical simulation for three cases: Spring, Autumn, and Winter were compared with the observational data obtained by ERM (Electrostatic Radon Monitor)[93] at Nagoya University. We should continue the numerical simulation until effects of the initial conditions fade away; we assumed the zero concentration thorough the whole areas initially. Since it took about 4 days for ^{222}Rn originated from the western boundary to arrive at Nagoya, the numerical simulation of ^{222}Rn transport for the least 5 days period was necessary until we got the reasonable results. The inflow of ^{222}Rn through horizontal and upper boundaries was assumed zero, because they were far enough from the observational point and the effects of boundary conditions were small.

The numerical simulation yielded a good fit for the case of Autumn but an overestimate for the cases of Spring and Winter. Fig. 5-7 shows the comparison of calculated values and observed ones for an example of Autumn.

Fig. 5-8 shows the average of observed and calculated ^{222}Rn concentrations where the components of local and regional parts are shown for calculated one. The magnitude of averaged ^{222}Rn concentration in each season is mainly occupied by the magnitude of the diurnal variation which comes from the local part.

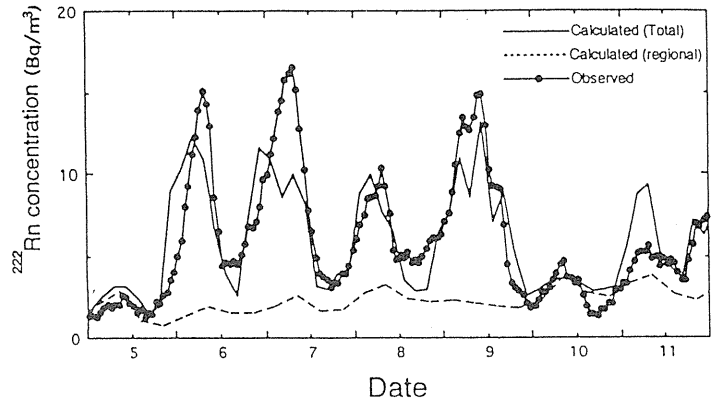

Fig. 5-7(a) Comparison of observed and calculated values, 1990.11.5—11.11.

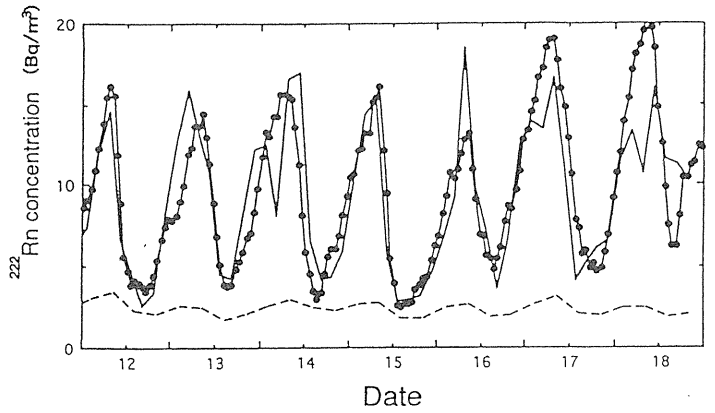

Fig. 5-7(b) Comparison of observed and calculated values, 1990.11.12—11.18.

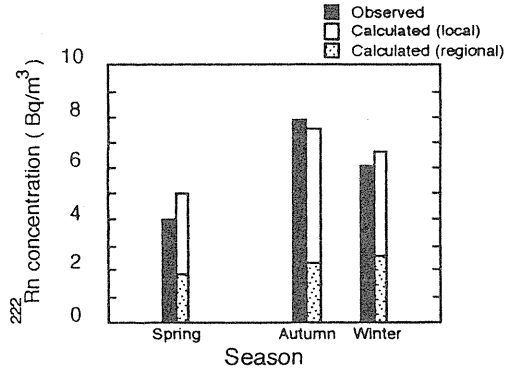

Fig. 5-8 Average of observed and calculated value in three seasons.

5.4 Conclusion

The time variation of atmospheric ^{222}Rn concentration was calculated by using a numerical model. Based on the results of numerical simulation of radon, we separate the ^{222}Rn concentration measured at Nagoya into the following two components : (1)^{222}Rn atom originated near from the measuring site, which is denoted by "diurnal variation component". From numerical simulation of radon, it has been shown that the measured diurnal variation can be explained by this component. (2)^{222}Rn atoms originated far from the measuring site (including Chinese Continent), which is denoted by "background component". For this component, we propose here a one layer transport model using air mass trajectory technique. By this model we can explain the temporal variation of background component.

The numerical calculation provided following conclusions.

(1) The variation of observed ^{222}Rn concentration agreed with that of calculated one.
(2) This study suggested that the magnitude of average ^{222}Rn concentration in each season was mainly affected by the contribution of local part.
(3) We obtained the best fit for the example of Autumn as for the ratio of observed and calculated ^{222}Rn concentrations.

This model will be applied to the transport of various pollutants.

6. Summary

To clarify the interaction between ^{218}Po ions and condensation nuclei, simultaneous measurements of the concentration of ^{218}Po ions (n_A), radon-222, and condensation nuclei (Z) were carried out at several stations. In some occasions, the diffusion coefficients of nuclei (D) were also measured. It was found that the correlation among them may be well expressed by the simple formula; $q_A=\beta_A n_A Z$. The correlation between β_A and D (or radius of nuclei) was also obtained. The variation of ^{222}Rn concentration was analyzed and the dependency of the ^{222}Rn concentration to the wind speed was theoretically explained. Turbulent diffusivities of the air close to the ground were obtained from thoron profiles.

A passive electrostatic integrating ^{222}Rn monitor was developed, which enabled us to obtain easily the regional distribution of ^{222}Rn in the Tokai District. A electrostatic radon monitor was also developed with which outdoor ^{222}Rn concentrations were measured continuously at six locations in Japan and China.

A three-dimensional numerical simulation was developed for calculating the temporal variation of ^{222}Rn. The variation of measured ^{222}Rn concentration agreed with that of calculated one.

Acknowledgement

The authors wish to express their sincere thanks to many students who worked with us for their invaluable cooperation in these research. The authors wish to thank Dr. M. Chino, Dr. H. Ishikawa and Dr. H. Yamazawa in JAERI for helps with developing the technique and method of analysis used in Chapter 4.

Reference

1) Israel, H. and Krebs, A., Nuclear Radiation in Geophysics, Spriger-Verlag, 1962.
2) Junge, C.E., Air Chemistry and Radioactivity, Academic Press, 1963.
3) Bricard, J., Girod, P. et Pradel, J., Radioactivite-Spectre de mobilite des petits ions radioactifs de l'air, C.R.Ac.Sc. **260**, 6587–6590, 1965.
4) Wilkening, M.H., Natural radioactivity as a tracer in the sorting of aerosols according to mobility, Rev. Sci. Instr. **23**, 13–16, 1952.
5) Wilkening, M.H., Kawano, M. and Lane, C., Radon-daughters ions and their relation to some electrical properties of the atmosphere, Tellus **18**, 679–683, 1966.
6) Chamberlain, A.C. and Dyson, E.D., The dose to the trachea and bronchi from the decay products of radon and thoron, Brit. Journ. Radiol, **29**, 317–326, 1955.
7) Kawano, M., Ikebe, Y., Nakashima, Y. and Shimizu, K., Some properties of naturally occurring radiations and radioactive ions in the atmosphere, Memoirs of the Faculty of Engineering, Nagoya Univ. **17**, 125–159, 1965.
8) Task Group on Lung Dynamics., Deposition and retention models for internal dosimetry of the human respiratory tract, Health Phys, **12**, 173–207, 1976.
9) Shimo, M., Torri, T. and Ikebe, Y., Measurements of unattached and attached RaA atoms in atmosphere and their deposition in human respiratory tract. J. At. Energy Soc. Japan **23**, 851–861, 1981.
10) ICRP. Limits for Inhalation of Radon Daughters by Workers., Publication 32 Ann. ICRP6, No.1, 1981.
11) Nolan, P.J. and Pollak, L.W., The calibration of a Photo-electric nucleus counter, Proc. Roy. Irish Acad. **51**, 9–31, 1946.
12) Nolan, J.J. and Guerrini, V.H., The diffusion coefficients and velocity of fall in air of atmospheric condensation nuclei, Proc. Roy. Irich Acad. **43**A2, 5–24, 1935.
13) Nolan, J.J. and Nolan, P.J., Diffusion and fall of atmospheric condensation nuclei, Proc. Roy, Irish Acad. **45**, 47–63, 1938.
14) Ikebe, Y., Estimation of vertical turbulent diffusivity from Tn profiles, Tellus, **24**, 29–37, 1972.
15) Keefe, K. and Nolan, P.J., Combination coefficients of ions and nuclei, Proc. Roy. Irish Acad. **62**, 43–53, 1962.
16) Ikebe, Y. and Kawano, M., Dependence of the effective attachment coefficient of small ions upon the size of condensation nuclei, Pure and Appl. Geophys. **83**, 120–130, 1970.
17) Lassen, L. and Rau, G., Die anlagerrung radioaktiver atome an aerosole (Schwebstoffe), Zeit. Physik **160**, 504–519, 1960.
18) James, A.C., Bradford, G.F. and Howell, D.M., Collection of unattached RaA atmos using a wire gauze., Aerosol Sci, 243–254, 1972.
19) George, A.C. and Hinchcliffe, L., Measurement of uncombined radon daughters in uranium mines., Health Phys, **23**, 791–803, 1972.
20) Duggan, M.J. and Howell, D.M., Relationship between the unattached fraction of airborne RaA and the concentration of condensation nuclei, Nature **224**, 1190–1191, 1969.
21) Fuchs, N.A., On the stationary charge distribution on aerosol particles in a bipolar ionic atmosphere, Geofis. Pura e Appl. **56**, 185–193, 1963.
22) Fuchs, N.A., The Mechanics of Aerosols, Pergamon, Oxford, 1964.
23) Shimo, M., The effective attachment coefficients of atmospheric ions and natural atoms to aerosol particles I, Res. Lett. Atmos. Electr., **5**, 55–64, 1985.
24) Shimo, M., The effective attachment coefficients of atmospheric ions and natural atoms to aerosol particles II, ibid., **5**, 65–71, 1985.
25) Hess, V.F. and Schmidt, W., Uber die Verteilung radioaktiver Gase in der freien Atmosphare., Physik. Zschr., **19**, 109–114, 1918.
26) Schmidt, W., Zur Verteilung radioaktiver Stoffe in der freien Luft. Physik. Zschr. **27**, 371–378., 1926.

27) Malakhov, S.G., Vertical distribution of radioactive emanation in the atmosphere., Izvest. Acad. Nauk S.S.S.R. Ser. Geopfiz., **9**, 1344–1351, 1959.
28) Jacobi, W. and Andre, K., The vertical distribution of radon-222, radon-220 and their decay products in the atmosphere., J. Geophys. Res., **68**, 3799–3814, 1963.
29) Israel, H., Horbert, M. and de la Riva, C., The thoroncontent of the atmosphere and its relation to the exchange conditions., Final Tech. Rept., European Research Office, U.S. Army Contract DA-91-591-EUC-3761, 1967.
30) Ikebe, Y., Variation of radon and thoron concentrations in relation to the wind speed., J. Meteor. Soc. Japan., **48**, 461–468, 1970.
31) Birot, A., Adrouger, B. and Fontan, J., Vertical distribution of radon 222 in the atmosphere and its use for study of exchange in the lower troposphere., J. Geophys. Res., **75**, 2373–2383, 1970.
32) Wilkening, M.H., Variation of natural radioactivity in the atmosphere with altitude, Trans. Amer. Geophy. Union., **37**, 177–180, 1956.
33) Hosler, C.R., Vertical diffusivity from radon profiles, J. Geophys. Res., **74**, 7018–7026.
34) Sisigina, T.L., Vertical distribution of radon in the boundary layer of the atmosphere (0–300 m) in connection with changing meteorological conditions, Izvest. Akad. Nauk S.S.S.R. Ser. Geofiz, **3**, 414–421, 1964.
35) Reiter, R., On radioactive equilibrium in atmospheric aerosols at 700 and 1800 m a.s.l., as influenced by particle size and vertical mixing activity, Pure Appl. Geophys. **74**, 134–150, 1969.
36) Crozier, W.D. and Biles, N., Measurements of radon 220 (thoron) in the atmosphere below 50 centimeters., J. Geophys. Res., **71**, 4735–4741, 1966.
37) Israël, H., Horbert, M. and de La Riva, C., Measurements of the thoron concentration of the lower atmosphere in relation to the exchange (austausch) in this region, Final. Tech. Rept, European Research Office, U.S. Army contract DAJA 37-67-c-0593, 1968.
38) Sutton, O.G., Micrometeorology, McGrwa-Hill, New York, 1953.
39) Ito, K., Atmospheric Pollution and It's Controll (in Japanese). Chijin-Shokan, Tokyo, 244, 1964.
40) Israel, H., Compendium of meteorology, Am. Meteorol. Soc., Boston, 155–161, 1951.
41) Wilkening, M.H. and Hand, J.E., Radon flux at the earth-air interface., J. Geophys. Res. **65**, 3367–3370.
42) Junge, C.E., Air. Chemistry and Radioactivity. Academic Press, New York and London, 1963.
43) Pearson, J.E. and Jones, G.E., Emanation of radon-222 from soils and its use as a tracer. J. Geophys. Res. **70**, 5279–5290, 1965.
44) Wilkenign, M.H., Clements, W.E. and Stankey, D., Radon-222 flux measurements in widely separated regions., The natural radiation environment II (eds. J.A.S. Adams et al.), USERDA CONF-720805, pp.717–730 (1972).
45) Crozier, W.D. and Biles, N., Measurements of radon 220 (thoron) in the atmosphere below 50 centimeters, J. Geophys. Res., **71**, 4735–4741, 1966.
46) Israel, H., Horbert, M. and de La Riva, C., Measurements of the thoron concentration of the lower atmosphere in relation to the exchange (Austausch) in this regon., Final Tech. Rept., European Research Office, U.S. Army, Contract, DAJA 37-67-0-0593, 1968.
47) Styra, B., Nedveckaite, T.N. and Senko, E.E., New methods of measuring thoron (radon 220) exhalation, J. Geophys. Res. **75**, 3635–3638, 1970.
48) Guedalia, D., Laurent, J.L., Fontan, J., Blanc, D. and Druilhet, A., A study of radon 220 emanation from soils, J. Geoophys. Res., **75**, 257–369, 1970.
49) Crozier, W.D., Direct measurement of radon 220 (thoron) exhalation from the ground, J. Geophys. Res., **74**, 4199–4205, 1969.
50) Deacon, E.L., Vertical diffusion in the lowest layer of the atmosphere, Quart. J. Roy. Meteor. Soc. **75**, 89–103, 1949.
51) Alter, H.W. and Fleischer, R.L., Passive integrating radon monitor for environmental monitoring. Health Phys., **40**, 693–702, 1981.
52) Urban M. and Piesch E., Low level environmental radon dosimetry with a passive track detector device. Radiat. Prot. Dosim., **1**, 97–109, 1981.
53) Bartlett, D.W., Gilvin, P.J., Dixon, D.W., Solanki, H.L. and Miles, J.C.H., The performance of the NRPB radon personal dosimeter. Radiat. Prot. Dosim., **17**, 139–142, 1986.

54) Put, L.W. and de Meijer, R.J., Variation of time-averaged outdoor radon concentrations over a distance of about 50 kilometers. Radiat. Prot. Dosim., **24**, 97–99, 1988.
55) Iida, T., Ikebe, Y., Hattori, T., Yamanishi, H., Abe, S., Ochifuji, K. and Yokoyama, S., An electrostatic integrating ^{222}Rn monitor with cellulose nitrate film for environmental monitoring. Health Phys., **54**, 139–148, 1988.
56) Abe, M. and Abe, S., Proceedings of the 15th NIRS Seminar on Environmental Research, Chiba, Japan, 1989, p.79 (in Japanese).
57) Yamanishi, H., Iida, T., Ikebe, Y., Abe, S. and Hata, T., Measurements of regional distribution of radon-222 concentration., J. Nucl. Sci. Technol., **28**, 331–338, 1991.
58) Jin, Y., Ikebe, Y., Iida, T., Shimo, M., Yamanishi, H., Guo, Q., Abe, S., Wang, Z., Ren, T., Tian, D., He, Z., Fan, X., Xie, H., Yang, X., Li, S., Lu, S., Zhang, H. and Du, K., Hoken Butsuri, **26**, 341 (1991) (in Japanese).
59) Iida, T., Ikebe, Y., Yamanishi, H., Abe, S. and Jin, Y., A survey of outdoor and indoor ^{222}Rn concentrations by passive method in Japan and China. Proc. Intern. Conf. on Rad. Effects and Protection, Mito, Japan, 1992, pp.364–369.
60) Jin, Y., Wang, Z., Iida, T., Ikebe, Y., Abe, S., Chen, H., Wu, L., Zeng, Q., Du, K. and Li, S., A new subnationwide survey of outdoor and indoor ^{222}Rn concentrations in Chine. Environ. Inter., **22**, S657–S663, 1996.
61) Busigin, A., van der Vooren, A.W., Babcock, J.C. and Phillips, C.R., The nature of unattached RaA (^{218}Po) particles. Health Phys., **40**, 333–343, 1981.
62) Currie, L.A., Limits for qualitative detection and quantitative determination. Anal. Chem., **40**, 586–593, 1968.
63) UNSCEAR United Nations Scientific Committee on the Effects of Atomic Radiation, Sources and effects of ionizing radiation. New York, UN, 1993, p.33–89.
64) Zhang, S., Pan, J., Li, R., Xu, C., Zhu, C., Wang, X. and Lou, R., Levels and distributions of radionuclides in soil in China. Chn. J. Radiat. Med. Prot., **8**, 1–15, 1988 (in Chinese).
65) Budnitz, R.J., Radon-222 and its daughters – A review of instrumentation for occupational and environmental monitoring. Health Phys., **26**, 145–164, 1974.
66) Lucas, H.F., Improved low-level alpha-scintillation counter for radon. Rev. Sci. Instrum., **28**, 680–683, 1957.
67) Thomas, J.W. and LeClare, P.C., A study of the two-filter for radon-222. Health Phys., **18**, 113–122, 1970.
68) Wrenn, M.E., Spitz, H. and Cohen, N., Design of a continuous digital-output environmental radon monitor. IEEE Trans. Nucl. Sci., **22**, 645–648, 1975.
69) Iida, T., An electrostatic radon monitor for the continuous measurement of environmental radon. Atmospheric radon families and environmental radioactivity edited by Okabe, Atomic Energy Soc. Jpn., 1985, p.65–73 (in Japanese).
70) Dua, S.K., Kotrappa, P. and Gupta, P.C., Influence of relative humidity on the charged fraction of decay products of radon and thoron. Health Phys., **45**, 152–157, 1983.
71) Iida, T. and Ikebe, Y., A low-energy beta-particle imaging system for measuring tritium distributions. Nucl. Instrum. Meth. **A253**, 119–127, 1986.
72) Shimo, M. and Guo, Q., On the deriving methods of counting efficiency with radon progeny. Hoken Butsuri, **29**, 33–39, 1994 (in Japanese).
73) Hopke, P.K., Use of electrostatic collection of ^{218}Po for measuring Rn., Health Phys., **57**, 39–42, 1989.
74) Currie, L.A., Limits for qualitative detection and quantitative determination. Anal. Chem., **40**, 586–593, 1968.
75) Ikebe, Y., Yamanishi, H., Tojo, K. and Iida, T., Relationship between radon exhalation rate from ground and atmospheric radon concentration. J. At. Energy Soc. Jpn., **35**, 735–738, 1993 (in Japanese).
76) Yamanishi, H., Iida, T., Ikebe, Y., Abe, S. and Hata, T., Measurements of regional distribution of radon-222 concentration. J. Nucl. Sci. Technol., **28**, 331–338, 1991.

77) Jin, Y., Ikebe, Y., Iida, T., Shimo, M., Yamanishi, H., Guo, Q., Abe, S., Wang, Z., Ren, T., Tian, D., He, Z., Fan, X., Xie, H., Yang, X., Li, S., Lu, S., Zhang, H. and Du, K., A survey of outdoor and indoor ^{222}Rn concentrations by passive method in China. Hoken Butsuri, **26**, 341–349, 1991 (in Japanese).
78) Rangarajan, C., Gopalakrishnan, S.S. and Eapen, C.D., The diurnal nad seasonal changes in short-lived radon-thoron daughters' concentrations in the coastal and inland regions of India and their possible relation to regional climatology, Pure Appl Geophys., **112**, 941–953, 1974.
79) Wilkening, M.H., Daily and annual courses of natural atmospheric radioactivity, J.G.R., **64**, 521–526, 1959.
80) Chino, M., Yamazawa, H. and Iida, T., Development of an atmospheric ^{222}Rn concentration model using a hydrodynamic meteorological model, Health phys., **70**, 47–54, 1996.
81) Sakashita, T., Murakami, T., Iida, T., Ikebe, Y., Chino, M. and Suzuki, K., Simulation of Diurnal Variation of Atmospheric ^{222}Rn Concentrations with Three-Dimensional Atmospheric Dispersion Model., J. Jpn. Health Phys. Soc., **31**, 161–168, 1996.
82) Ikebe, Y., Kojima, S. and Shimo, M., On the origin and transport of Rn-222 in the atmosphere, Res. Lett. Atmos. Electr., Vol.3, 51–54, 1983.
83) Misaki, M., Ikegami, M. and Kanazawam I., Deformation of the size distribution of aerosol particles dispersing from land to ocean, J. Meteor. Soc. Japan, **53**, 111–120, 1975.
84) Mochizuki, T. and Tanji, T., Radioactive Aerosols in the Southern Ocean of Japan Island, Res. Lett. Atmos. Electr., **1**, 9–14, 1981.
85) Turekian, K.K., Nozaki, Y. and Benninger, L.K., Geochemistry of atmospheric radon and radon products, Ann. Rev. Earth Planet. Sci., **5**, 227–255. 1977.
86) Wilkening, M.H. et al., The Nat. Radiat. Env. II, ed. I.A.S. Adams, 2 : 717–30, USERDA CONF-720805, 1972.
87) Ishikawa, H. and Chino, M., Development of regionally extended/Worldwide version of system for prediction of environmental emergency dose information : WSPEEDI, (II), J. Nucl. Sci. and Technol., **28**, 642–655, 1991.
88) Ishikawa, H., Development of regionally extended/Worldwide version of system for prediction of environmental emergency dose in formation : WSPEEDI, (I), Nucl. Sci. and Technol., **28**, 535–546, 1991.
89) Maekawa, I., Numerical diffusion in multi-dimensional thermal-hydraulic analysis, (II), J. Atomic Energy Soc. of Japan, **29**, 823–833, 1987.
90) Diehl, S.R., Smith, D.T. and Syor, M., Random-walk simulation of gradient-transfer processes applied to dispersion stack emission from coal-fired power plants, J. of Appl. Meteor., **21**, 69–83, 1982.
91) Smith, G.D., Numerical solution of particle differential equations, P.17. Oxford University Press, Oxford, 1965.
92) Mellor, G. and Yamada, T., A simulation of wangara atmospheric boundary layer data, J. of Atmos. Sci., **31**, 1791–1805, 1974.
93) Iida, T., Ikebe, Y. and Tojo, K., An electrostatic radon monitor for measurement of environmental radon., Res, Lett. Atmos. Electr., **11**, 55–59, 1991.